IOP Publishing and International Atomic Energy Agency Nuclear Fusion
Nucl. Fusion **53** (2013) 043011 (18pp) doi:10.1088/0029-5515/53/4/043011

Extension of neoclassical rotation theory for tokamaks to realistically account for the geometry of magnetic flux surfaces

C. Bae[1,a], **W.M. Stacey**[1] **and W.M. Solomon**[2]

[1] Fusion Research Center, Georgia Institute of Technology, Atlanta, GA 30332, USA
[2] Princeton Plasma Physics Laboratory, Princeton, NJ 08540, USA

E-mail: cbae@nfri.re.kr

Received 25 September 2012, accepted for publication 14 February 2013
Published 19 March 2013
Online at stacks.iop.org/NF/53/043011

Abstract
A neoclassical rotation theory (poloidal and toroidal) is developed from the fluid moment equations, using the Braginskii decomposition of the viscosity tensor extended to generalized curvilinear geometry and a neoclassical calculation of the parallel viscosity coefficient interpolated over collision regimes. Important poloidal dependences are calculated using the Miller equilibrium flux surface geometry representation, which takes into account elongation, triangularity, flux surface compression/expansion and the Shafranov shift. The resulting set of eight (for a two-ion-species plasma model) coupled nonlinear equations for the flux surface averaged poloidal and toroidal rotation velocities and for the up–down and in–out density asymmetries for both ion species are solved numerically. Comparison of prediction with measured carbon poloidal and toroidal rotation velocities in a co-injected and a counter-injected H-mode discharge in DIII-D (Luxon J. 2002 *Nucl. Fusion* **42** 614) indicates agreement to within $<10\%$ except in the very edge ($\rho > 0.90$) in the co-injected discharge.

(Some figures may appear in colour only in the online journal)

1. Introduction

Rotation of tokamak plasmas is known to be important for the stabilization of magnetohydrodynamics (MHD) instabilities and for achieving good confinement in tokamaks, as well as providing insight about transport. Earlier studies indicated that toroidal rotation affects neoclassical particle transport to suppress the MHD instabilities [1–4] and is postulated to play a role in the shear suppression of microinstabilities that enhance transport [5]. Because of the importance of characterizing and understanding toroidal rotation and the related angular momentum transport in neutral beam driven tokamaks, there has been a longstanding effort both experimentally [6–11] and theoretically [12–28] to understand and predict toroidal rotation, but this task has been challenging. Poloidal rotation is also of interest because of its role in the shear suppression of turbulent energy transport [5].

In understanding toroidal rotation and the angular torque mechanisms, representation of the viscosity stress is very important. From the earlier classical studies in cylindrical geometry [9, 15, 16], the familiar perpendicular viscosity was calculated to be too small to account for the observed momentum damping. Taking neoclassical effects into account [15, 16, 19, 20] did not change this result, leading to the belief that the momentum transport in tokamak plasmas must be due to an 'anomalous' effect. For clarification, in this paper 'neoclassical' refers to the classical transport plus the transport due to toroidal geometry (i.e. Pfirsch–Schluter (PS) transport) and trapped particle effects.

What generally has not been accounted for in these early neoclassical studies [15, 16, 19, 20] is the GYROVISCOUS contribution to the radial angular momentum transport, which is larger than the PERPENDICULAR viscosity component by several orders of magnitude when significant up–down asymmetries are present [13, 14]. This gyroviscous contribution vanishes in classical cylindrical geometry and appears only at a higher gyroradius order in neoclassical theories. Even more advanced neoclassical theories [19, 20, 26] which do not treat poloidal dependences (geometric expansion and compression) of density and velocity in the formalism failed to properly calculate the gyroviscous transport contribution, but recovered only the much smaller perpendicular viscosity. However, there exist several theoretical studies [13, 14, 17, 18, 21–25, 27–29] that have provided a firm theoretical basis for the importance of gyroviscosity relative to perpendicular viscosity.

Motivated by the indicated importance of neoclassical gyroviscosity, studies with a simple circular flux surface

[a] Author to whom any correspondence should be addressed.

geometry (the 'circular model' [12, 30–33]) were previously carried out to calculate toroidal velocity and the related gyroviscous momentum transport, taking into account density and velocity asymmetries in the formalism. These studies established that gyroviscosity predicts the right order of magnitude of the toroidal velocity, thus demonstrating the greater importance of the gyroviscous contribution relative to the much smaller perpendicular transport. The calculated carbon toroidal velocities, however, were about a factor of two larger (e.g. [30]) than the experimental measurement, indicating either that the approximations in the representation of important poloidal asymmetries made in the 'circular gyroviscous model' were too crude or that other equally significant momentum transport mechanisms must be present, or both.

One gross approximation in the circular model studies [12, 30–33] is believed to be the representation of the actual D-shaped equilibrium flux surfaces with a circular geometry, which limits the accuracy of the calculation of poloidal dependences of density and velocity. In these previous studies, it was shown that the angular momentum transport rates are strong functions of these poloidal asymmetries. Thus, without a more accurate representation of the poloidal dependences along the flux surfaces, it was not possible to determine how well neoclassical theory could predict rotation. This observation has motivated the development of a new neoclassical plasma rotation theory based on the more accurate flux surface geometry given by the Miller equilibrium flux surface geometry (the 'Miller model' hereafter) [34] that became available in 1998 [35, 36].

The main objectives of this paper are (i) to present the theoretical development of a new neoclassical plasma rotation and transport theory based on the Miller model representation of poloidal asymmetries, and (ii) to compare the calculated poloidal and toroidal rotation velocities with measurements made in two recent DIII-D discharges [37]. The implication of the results to the general question of the adequacy of neoclassical rotation calculations in accounting for rotation in tokamaks is discussed.

2. Plasma fluid equations

The motions of charged particles in plasmas are governed by the continuity, momentum balance, and energy balance equations shown below with 'j' being species (ions or electrons).

Continuity equation:

$$\frac{\partial n_j}{\partial t} + \nabla \cdot (n_j \vec{V}_j) = S_j^o. \tag{1}$$

Momentum balance equation:

$$m_j \frac{\partial}{\partial t}(n_j \vec{V}_j) + m_j \nabla \cdot (n_j \vec{V}_j \vec{V}_j) + \nabla p_j + \nabla \cdot \overleftrightarrow{\mathbf{\Pi}}_j = n_j e_j (\vec{E} + \vec{V}_j \times \vec{B}) + \vec{F}_j^1 + \vec{S}_j^1. \tag{2}$$

Energy balance equation:

$$\frac{\partial}{\partial t}\left(\frac{1}{2}\mathrm{Tr}\, M_j\right) + \nabla \cdot \left(\frac{1}{2} n_j m_j V_j^2 \vec{V}_j + \frac{5}{2} n_j T_j \vec{V}_j + \overleftrightarrow{\mathbf{\Pi}}_j \cdot \vec{V}_j + \vec{q}_j\right) = n_j e_j \vec{V}_j \cdot \vec{E} + F_j^2 + S_j^2, \tag{3}$$

where $\mathrm{Tr}\, M_j$ is the scalar trace of the momentum stress tensor

$$\overleftrightarrow{M}_j \equiv n_j m_j \langle \vec{V}_j \vec{V}_j \rangle_j = n_j m_j \vec{V}_j \vec{V}_j + p_j \overleftrightarrow{I} + \overleftrightarrow{\mathbf{\Pi}}_j, \tag{4}$$

$\vec{F}_j$ is the friction, and $\vec{q}_j = -n_j \chi_j \nabla T_j$ is the heat conduction relation. The first and second term in the momentum balance equation (2), can be expanded as

$$m_j \frac{\partial}{\partial t}(n_j \vec{V}_j) = m_j \vec{V}_j \frac{\partial n_j}{\partial t} + n_j m_j \frac{\partial \vec{V}_j}{\partial t}, \tag{5}$$

$$m_j \nabla \cdot (n_j \vec{V}_j \vec{V}_j) = n_j m_j (\vec{V}_j \cdot \nabla) \vec{V}_j + m_j \vec{V}_j \nabla \cdot (n_j \vec{V}_j). \tag{6}$$

When multiplying the continuity equation by $m_j \vec{V}_j$, we obtain

$$m_j \vec{V}_j \frac{\partial n_j}{\partial t} = m_j \vec{V}_j S_j^o - m_j \vec{V}_j \nabla \cdot (n_j \vec{V}_j) \tag{7}$$

which when replacing the first term in equation (5) its second term cancels out the second term in equation (6), thus yielding the basic form of the momentum balance equation used in this research:

$$n_j m_j \frac{\partial \vec{V}_j}{\partial t} + n_j m_j (\vec{V}_j \cdot \nabla) \vec{V}_j + \nabla p_j + \nabla \cdot \overleftrightarrow{\mathbf{\Pi}}_j = n_j e_j (\vec{E} + \vec{V}_j \times \vec{B}) + \vec{F}_j^1 + \vec{S}_j^1 - m_j \vec{V}_j S_j^o. \tag{8}$$

The viscosity tensor ($\overleftrightarrow{\mathbf{\Pi}}_j$) can be represented in (at least) two different ways by different ordering arguments. The short mean free path (i.e. highly collisional or PS) description of viscosity, originally formulated by Braginskii [14], assumes a 'strong rotation' ordering in which ion mean flow is on the order of ion thermal speed, $|V_\perp| \ll |V_\parallel| \sim V_{\mathrm{thi}}$ where V_{thi} is the ion thermal velocity. Mikhailovskii and Tsypin [17] realized that this ordering is not one of the most interest in many practical situations, as in the plasma edge region or in discharges with low rotation, and assumed ion mean flow to be on the order of the diamagnetic drift velocity, thus $|V_\parallel| \ll V_{\mathrm{thi}}$ in this 'weak rotation' ordering. In reducing the plasma fluid equations to derive a neoclassical plasma rotation theory, either Braginskii's or Mikhilovskii's viscosity formalism may be employed if the corresponding ordering conditions are satisfied. For this research, we limit the scope of the research to Braginskii's ordering since it is valid for strongly rotating tokamak plasmas heated with directed neutral beam injection, except in the edge region. Using this ordering will enable us to check the validity of the new plasma rotation theory against measurements with significant rotation, presumably involving less experimental uncertainty. The extension of the present theory to Mikhailovskii's ordering is a useful topic for future research.

Applying Braginskii's viscosity formalism to axisymmetric ($\partial/\partial\phi = 0$) toroidal flux surface geometry [18], which is eventually the 'PS' extension of classical gyroviscosity, the steady-state plasma fluid equations are reduced to equations (9)–(12). Note that the momentum balance equation is

composed of three scalar components (r, θ, ϕ) and that the energy balance equation is not needed in this study with Braginskii's ordering (but would be included in future weak rotation studies).

Continuity equation:

$$\frac{1}{h_r}\frac{\partial}{\partial r}(n_j V_{rj}) + \frac{n_j V_{rj}}{h_r}\left(\frac{1}{h_\phi}\frac{\partial h_\phi}{\partial r} + \frac{1}{h_\theta}\frac{\partial h_\theta}{\partial r}\right) + \frac{1}{h_\theta}\frac{\partial}{\partial \theta}(n_j V_{\theta j}) + \frac{n_j V_{\theta j}}{h_\theta}\left(\frac{1}{h_\phi}\frac{\partial h_\phi}{\partial \theta} + \frac{1}{h_r}\frac{\partial h_r}{\partial \theta}\right) = n_e(n_{oj}\langle\sigma V\rangle_{\mathrm{ion}\,j}) \equiv n_e \nu_{\mathrm{ion}\,j}. \quad (9)$$

Radial momentum balance equation:

$$n_j m_j[(\vec{V}_j\cdot\nabla)\vec{V}_j]_r + \frac{1}{h_r}\frac{\partial p_j}{\partial r} + (\nabla\cdot\overleftrightarrow{\mathbf{\Pi}}_j)_r = n_j e_j(E_r + V_{\theta j}B_\phi - V_{\phi j}B_\theta) + F_{rj} + (S^1_{rj} - m_j V_{rj} S^0_j). \quad (10)$$

Poloidal momentum balance equation:

$$n_j m_j[(\vec{V}_j\cdot\nabla)\vec{V}_j]_\theta + \frac{1}{h_\theta}\frac{\partial p_j}{\partial \theta} + (\nabla\cdot\overleftrightarrow{\mathbf{\Pi}}_j)_\theta = n_j e_j(E_\theta - V_{rj}B_\phi) + F_{\theta j} + (S^1_{\theta j} - m_j V_{\theta j} S^0_j). \quad (11)$$

Toroidal momentum balance equation:

$$n_j m_j[(\vec{V}_j\cdot\nabla)\vec{V}_j]_\phi + (\nabla\cdot\overleftrightarrow{\mathbf{\Pi}}_j)_\phi = n_j e_j(E^A_\phi + V_{rj}B_\theta) + F_{\phi j} + (S^1_{\phi j} - m_j V_{\phi j} S^0_j), \quad (12)$$

where h_r, h_θ and h_ϕ are differential metric coefficients (or scale factors) for a given flux surface geometry, which relate differential coordinates and their length elements by $\mathrm{d}l_r = h_r\,\mathrm{d}r$, $\mathrm{d}l_\theta = h_\theta\,\mathrm{d}\theta$ and $\mathrm{d}l_\phi = h_\phi\,\mathrm{d}\phi$. E^A_ϕ is the toroidal component of the inductive electric field $\vec{E}^A = -\partial\vec{A}/\partial t$. Details of representing the plasma fluid equations in general curvilinear geometry has been worked out earlier [36]. All coordinate components of the inertial term, $[(\vec{V}\cdot\nabla)\vec{V}]$, and the viscous term, $(\nabla\cdot\overleftrightarrow{\mathbf{\Pi}})$, can be found in appendix A.

To acquire relations required to solve for rotation velocities and poloidal asymmetries, further approximations are made to equations (9)–(12) by introducing the strong rotation ordering to eliminate negligible terms. We start by neglecting radial velocities because $V_r \ll V_\theta < V_\phi \sim V_{\mathrm{th}}$ holds in tokamak plasmas in the strong rotation ordering. The continuity equation then becomes

$$\frac{1}{h_r}\frac{\partial}{\partial r}(n_j V_{rj}) + \frac{1}{h_\theta}\frac{\partial}{\partial \theta}(n_j V_{\theta j}) + \frac{n_j V_{\theta j}}{h_\theta}\left(\frac{1}{h_\phi}\frac{\partial h_\phi}{\partial \theta} + \frac{1}{h_r}\frac{\partial h_r}{\partial \theta}\right) = n_e \nu_{\mathrm{ion}\,j}. \quad (13)$$

Assuming that all other terms except the pressure gradient and electromagnetic force terms are negligible, the radial momentum balance equation reduces to

$$\frac{1}{h_r}\frac{\partial p_j}{\partial r} = n_j e_j(E_r + V_{\theta j}B_\phi - V_{\phi j}B_\theta) = n_j e_j\left(-\frac{1}{h_r}\frac{\partial \Phi}{\partial r} + V_{\theta j}B_\phi - V_{\phi j}B_\theta\right), \quad (14)$$

where Φ is the electrostatic potential. In the poloidal momentum balance equation (11), the inertial and viscous terms from appendix A reduce to

$$[(\vec{V}\cdot\nabla)\vec{V}]_\theta = \frac{V_{\theta j}}{h_\theta}\frac{\partial V_{\theta j}}{\partial \theta} - \frac{V_{\theta j}V_{\phi j}}{h_\theta h_\phi}\frac{\partial h_\phi}{\partial \theta}, \quad (15)$$

$$(\nabla\cdot\Pi)_\theta = \frac{1}{H}\frac{\partial}{\partial r}(Rh_\theta\Pi_{r\theta}) + \frac{1}{H}\frac{\partial}{\partial \theta}(h_r h_\phi \Pi_{\theta\theta}) - \frac{1}{h_\theta h_r}\frac{\partial h_r}{\partial \theta}\Pi_{rr} + \frac{1}{h_\theta h_r}\frac{\partial h_\theta}{\partial r}\Pi_{\theta r} - \frac{1}{Rh_\theta}\frac{\partial R}{\partial \theta}\Pi_{\phi\phi}, \quad (16)$$

where $H = h_r h_\theta h_\phi$. In the toroidal momentum balance equation (12), the inertial and viscous terms in appendix A reduce to

$$[(\vec{V}\cdot\nabla)\vec{V}]_\phi = \left(\frac{V_{rj}}{h_r}\frac{\partial V_{\phi j}}{\partial r} + \frac{V_{\phi j}V_{rj}}{h_\phi h_r}\frac{\partial h_\phi}{\partial r}\right) + \left(\frac{V_{\theta j}}{h_\theta}\frac{\partial V_{\phi j}}{\partial \theta} + \frac{V_{\phi j}V_{\theta j}}{h_\phi h_\theta}\frac{\partial h_\phi}{\partial \theta}\right), \quad (17)$$

$$(\nabla\cdot\Pi)_\phi = \left[\frac{1}{Rh_\theta h_r}\frac{\partial}{\partial r}(Rh_\theta\Pi_{r\phi}) + \frac{1}{Rh_r}\frac{\partial R}{\partial r}\Pi_{r\phi}\right] + \left[\frac{B_\theta}{h_\theta}\frac{\partial}{\partial \theta}\left(\frac{\Pi_{\theta\phi}}{B_\theta}\right) + \frac{1}{Rh_\theta}\frac{\partial R}{\partial \theta}\Pi_{\theta\phi}\right]. \quad (18)$$

These reduced forms of the continuity and momentum balance equations constitute the basic set of relations required to develop any plasma rotation theory in strongly rotating plasmas. In this study, a neoclassical plasma rotation theory is developed for a two-species 'deuterium-carbon' plasma for simplicity but can also be extended to multiple ion species by summing over all ion species to calculate the friction term and the electron density from charge neutrality.

2.1. Extended Stacey–Sigmar plasma poloidal rotation model

Quite different plasma poloidal rotation theories can be developed from the same basic set of equations in the previous section, based on which terms are retained in the momentum balance equations and how the viscosity and poloidal dependences of density and velocity are represented in equations (10)–(12). One of the biggest differences among existing theories is the number of terms retained in the poloidal momentum balance, equation (11). Such differences in poloidal rotation calculation models ultimately affect the toroidal velocity calculations. One of the early poloidal rotation models is based on the Hirshman–Sigmar poloidal rotation theory (the H–S model) [38], which neglects all terms except the viscosity and friction terms, which are treated with a sophisticated friction and viscosity representation. This model is used in the NCLASS code [39]. The model by Kim, Diamond and Groebner (the KDG model) [40] is a trace-impurity approximation to the H–S model. The Shaing–Sigmar–Stacey (the S–S–S) model [1] retains more terms in the poloidal momentum balance equation and calculates poloidal density asymmetries to represent poloidal dependences. The most recent form of neoclassical poloidal rotation theory evolved from the S–S–S model is the Stacey–Sigmar poloidal rotation model (the 'S–S model' hereafter) [21, 30, 41], which uses the generalized curvilinear form of Braginskii's flow rate-of-strain tensor (see appendix A) [36, 42] and retains all terms to obtain

$$n_j m_j[(\vec{V}_j\cdot\nabla)\vec{V}_j]_\theta + (\nabla\cdot\overleftrightarrow{\mathbf{\Pi}}_j)_\theta + \frac{1}{h_\theta}\frac{\partial p_j}{\partial \theta} - M_{\theta j} + n_j m_j \nu_{jk}(V_{\theta j} - V_{\theta k}) + n_j e_j(V_{rj}B_\phi - E_\theta) + n_j m_j \nu_{\mathrm{ion}\,j} V_{\theta j} + n_j m_j \nu_{\mathrm{elcx}\,j} V_{\theta j} = 0, \quad (19)$$

which is basically equation (11) rewritten with the source and friction terms replaced with actual calculation models. The third term in equation (19) is the pressure gradient. The fourth term ($M_{\theta j}$) represents any external poloidal momentum input or torque and comes from representing the momentum source term as the momentum input minus momentum damping due to charge exchange and elastic scattering of rotating ions with non-rotating neutrals, as in

$$\vec{S}_j^1 = \vec{M}_j - n_j m_j \nu_{\mathrm{elex}\,j} \vec{V}_j. \tag{20}$$

The fifth term is the interspecies collisional friction, and a simple Lorentz form, $\vec{F}_j^1 = -n_j m_j \sum_k \nu_{jk}(\vec{V}_j - \vec{V}_k)$, is used in this study. The sixth term is a combination of $\vec{V} \times \vec{B}$ force and electric field force, the seventh term comes from the right-hand side of equation (13), and the last term comes from the second term in equation (20). This S–S model also replaces the parallel viscosity coefficient in the H–S model with the Shaing banana-plateau-PS viscosity interpolation formula $\langle \boldsymbol{B} \cdot \nabla \cdot \Pi_j \rangle = 3\langle (\boldsymbol{n} \cdot \nabla B)^2 \rangle \eta_{0j} (\boldsymbol{V}_{\theta j} \cdot \boldsymbol{B})/B^2$, where $\boldsymbol{n}$ is the unit vector in the magnetic field direction and

$$\eta_{0j} = \frac{n_j m_j V_{\mathrm{th}\,j} q R_0 \varepsilon^{-3/2} \nu_{jj}^*}{(1 + \varepsilon^{-3/2}\nu_{jj}^*)(1 + \nu_{jj}^*)} \equiv n_j m_j V_{\mathrm{th}\,j} q R f_j(\nu_{jj}^*) \tag{21}$$

and where the normalized collision frequency is $\nu_{jj}^* \equiv \nu_{jj} q R_0 / V_{\mathrm{th}\,j}$ with ν_{jj} being the self-collision frequency of species 'j', q is the safety factor, and $\varepsilon \equiv r/R_0$ [18, 42].

In the S–S poloidal rotation model, the poloidal dependences of density and velocity over flux surfaces are represented by the following low-order Fourier expansion:

$$n_j(r,\theta) \approx \overline{n}_j(r)[1 + n_j^{\mathrm{c}}(r)\cos\theta + n_j^{\mathrm{s}}(r)\sin\theta], \tag{22a}$$

$$V_j(r,\theta) \approx \overline{V}_j(r)[1 + V_j^{\mathrm{c}}(r)\cos\theta + V_j^{\mathrm{s}}(r)\sin\theta], \tag{22b}$$

where the overbar indicates the average values over flux surfaces, the cosine asymmetries with superscript 'c' represent 'in–out' variations, and the sine asymmetries with superscript 's' represents 'up–down' asymmetries. It should be noted that the poloidal variation of the flux surfaces will be represented by the Miller model, and any further poloidal variation of the density and flows will be represented by equations (22*a*) and (22*b*). This low-order Fourier representation should be adequate to pick up the leading order up–down and in–out component of any further asymmetries of the densities and flows over the flux surface. It would be conceptually straightforward to extend the formalism to include higher order Fourier expansions, but since this would be algebraically and computationally difficult we will defer this until there is evidence of the necessity to do so.

The electrostatic potential is also expanded in the form of equations (22*a*) and (22*b*) and, in principle, the ion and electron temperatures could be as well. However, we will argue that the large parallel thermal conductivities make a significant variation in temperature over the flux surface unlikely, which should certainly be true for the electrons. Calculation of the poloidal variation of the ion temperature would require use of the heat balance and heat conduction equations, which would greatly complicate the formalism, and this possibility will be deferred until a later paper. More details on the S–S poloidal rotation model can be found in [18, 42].

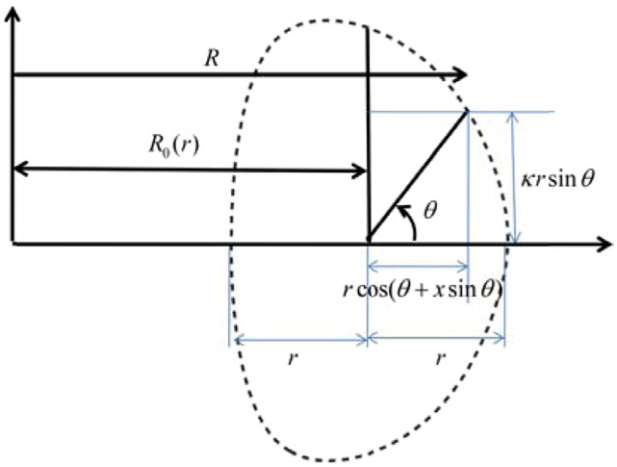

Figure 1. Miller equilibrium flux surface geometry.

Earlier studies with the S–S model [12, 30–33] have developed a neoclassical plasma rotation theory based on the circular flux surface geometry, and these previous calculations were compared to actual velocity measurements [30]. Although the calculated toroidal velocities were off by about a factor of two, these studies proved the possibility of using simple analytic flux surface geometry models in this type of neoclassical rotation and the related momentum transport calculations but concluded that higher accuracy could be achieved with a more accurate flux surface geometry since poloidal asymmetries are closely related to the geometric expansion, compression, and elongation of flux surfaces [30]. These findings have motivated the use of the Miller flux surface geometry to rederive a plasma rotation theory [35] based on the S–S poloidal rotation model.

2.2. *Miller equilibrium flux surface model*

The circular model was rather simpler in terms of the derivation and numerical coding but lacks the accuracy in the representation of poloidal dependences along the flux surfaces. Miller *et al* [34] presented an analytical geometry to better describe actual D-shaped equilibrium flux surfaces of tokamak plasmas with elongation κ and triangularity δ as shown in figure 1, thus one of the most advanced analytic representations of tokamak plasmas. $R_0(r)$ is a function of r, the half-diameter from the centre of plasma along the plasma mid-plane, representing the shifts of the centre of each flux surface. The R and Z coordinates of the Miller model are described by

$$R(r) = R_0(r) + r\cos(\theta + x\sin\theta) \equiv R_0(r) + r\cos\xi, \tag{23a}$$

$$Z(r) = \kappa r \sin\theta, \tag{23b}$$

where $x \equiv \sin^{-1}\delta$ and $\xi \equiv \theta + x\sin\theta$.

Analysis of the curvilinear differential geometry in all coordinates (r, θ, ϕ) yields the following metric coefficients for the Miller model [34, 35, 43]:

$$h_r = \left[\kappa\left[\cos(x\sin\theta) + \frac{\partial R_0(r)}{\partial r}\cos\theta + [s_\kappa - s_\delta\cos\theta + (1 + s_\kappa)x\cos\theta]\sin\theta\sin\xi\right]\right] \times \left[\sqrt{\sin^2\xi(1 + x\cos\theta)^2 + \kappa^2\cos^2\theta}\right]^{-1}, \tag{24}$$

$$h_\theta = \left[r\kappa \left[\cos(x\sin\theta) + \frac{\partial R_0(r)}{\partial r}\cos\theta + [s_\kappa - s_\delta\cos\theta + (1+s_\kappa)x\cos\theta]\sin\theta\sin\xi \right] \right] \times \left[\sqrt{\left(\frac{\partial R_0}{\partial r} + \cos\xi - s_\delta\sin\xi\sin\theta \right)^2 + \kappa^2\sin^2\theta(s_\kappa+1)^2} \right]^{-1}, \quad (25)$$

$$h_\phi = R(r) = R_0(1+\varepsilon\cos\xi), \quad (26)$$

where $s_\kappa(r) = (r/\kappa)(\partial\kappa/\partial r)$ and $s_\delta(r) = r(\partial\delta/\partial r)/\sqrt{(1-\delta^2)}$ account for the changes in elongation and triangularity respectively along the radial direction. Ampere's law provides the following magnetic field representations for the Miller model:

$$B_\theta(r,\theta) = \left(1 + \frac{\partial R_0(r)}{\partial r}\right)\frac{\overline{B}_\theta}{h_r(1+\varepsilon\cos\xi)}, \quad (27)$$

$$B_\phi = \frac{\overline{B}_\phi}{1+\varepsilon\cos\xi}. \quad (28)$$

With this analytical Miller model, we can use the S–S plasma poloidal rotation model to calculate the poloidal dependences of density and velocity represented in equations (22*a*) and (22*b*) more accurately, ultimately increasing the accuracy in the toroidal velocity and momentum transport calculations.

Different flux surface geometries provide different formulas for the flux surface average (FSA) calculations. For the Miller model, we have

$$\langle A(r,\theta)\rangle \equiv \frac{\oint \frac{A(r,\theta)\,\mathrm{d}\ell_\theta}{B_\theta}}{\oint \frac{\mathrm{d}\ell_\theta}{B_\theta}} = \frac{\oint A(r,\theta)Y(r,\theta)\,\mathrm{d}\theta}{\oint Y(r,\theta)\,\mathrm{d}\theta}, \quad (29a)$$

where

$$Y(r,\theta) = \left[(1+\varepsilon\cos\xi)\left[\cos(x\sin\theta) + \frac{\partial R_0(r)}{\partial r}\cos\theta + [s_\kappa - s_\delta\cos\theta + (1+s_\kappa)x\cos\theta]\sin\theta\sin\xi \right]^2 \right] \times \left[\left[\left[\left(\frac{\partial R_0}{\partial r} + \cos\xi - s_\delta\sin\xi\sin\theta \right)^2 + \kappa^2\sin^2\theta(s_\kappa+1)^2 \right][\sin^2\xi(1+x\cos\theta)^2 + \kappa^2\cos^2\theta] \right]^{1/2} \right]^{-1}. \quad (29b)$$

Unlike those of the circular model used in earlier studies [12, 30–33], FSAs in the Miller model do not reduce to simple analytic forms, thus must be numerically computed separately and imported into the final computation code. Note here that the circular model is simply a special case of the Miller model with elongation $\kappa = 1$, triangularity $\delta = 0$ and no Shafranov shift. This simple fact served as one of the tools to check the accuracy and validity of the new plasma rotation theory against the earlier circular model [12, 30] (see appendix B for revised circular model formalism) and for the numerical coding in this work.

3. Plasma rotation theory in the Miller model representation

3.1. Angular toroidal torques and transport with the Miller model

Now with all theoretical backgrounds required to develop a new neoclassical plasma rotation theory with the Miller geometry presented, we are ready to derive the formalism for calculating toroidal velocity and neoclassical gyroviscous contribution to angular momentum damping. The strong rotation ordering $V_r \ll V_\theta < V_\phi \sim V_{\mathrm{th}}$ is used. Earlier studies with the circular model [12, 30–33] now become special cases of this new theory. Thus, the new theory with the Miller model was developed in a similar fashion to the circular model theory [30] so that direct comparison would be possible to enable evaluation of the accuracy improvement. In this section, derivation of the toroidal angular torque formalism is presented first to stress the importance of the gyroviscous contribution to the total viscous torque.

From the first term of the toroidal momentum balance equation (12), the FSA of toroidal angular 'inertial' torque formalism using the Miller model is given by

$$\langle n_j m_j R^2\nabla\phi\cdot(\vec{V}_j\cdot\nabla)\vec{V}_j\rangle = R_0\overline{n}_j m_j \nu_{nj}\overline{V}_{\phi j} \quad (30)$$

with the 'inertial' transport frequency (ν_{nj}) given by

$$\nu_{nj} = \frac{\overline{V}_{rj}}{R_0}\left[\frac{\partial R_0}{\partial r}\left\langle\frac{1}{h_r}\right\rangle + \left\langle\frac{\cos\xi}{h_r}\right\rangle + \varepsilon\left(\widetilde{n}_j^c + \widetilde{V}_{\phi j}^c\right)\left\langle\cos\theta\frac{\cos\xi}{h_r}\right\rangle - R_0 L_{\overline{V}_\phi}^{-1}\right] + \overline{V}_{\theta j}\varepsilon\widetilde{V}_{\phi j}^s\left(\left\langle\cos\theta\frac{1}{h_\theta}\right\rangle + \frac{\left\langle\frac{1}{R}\frac{\partial R}{\partial\theta}\sin\theta\frac{1}{h_\theta}\right\rangle}{\left\langle\sin^2\theta\frac{1}{h_\theta}\right\rangle}\left\langle\cos^2\theta\frac{1}{h_\theta}\right\rangle + \varepsilon\left\langle\cos\theta\frac{\cos\xi}{h_\theta}\right\rangle + \frac{1}{R_0}\left\langle\frac{\partial R}{\partial\theta}\sin\theta\frac{1}{h_\theta}\right\rangle\right) \quad (31)$$

where $L_X^{-1} = -(1/X)(\partial X/\partial r)$ is the gradient length scale for a given quantity X, $\widetilde{n}_j^{s,c} = n_j^{s,c}/\varepsilon$, and $\widetilde{V}_{\phi j}^{c,s} \equiv V_{\phi j}^{c,s}/\varepsilon$.

Also from the second term of the toroidal momentum balance equation (12), the FSA of toroidal angular 'viscous' torque formalism is given by

$$\langle R^2\nabla\phi\cdot\nabla\cdot\overleftrightarrow{\Pi}\rangle = \langle(R^2\nabla\phi\cdot\nabla\cdot\overleftrightarrow{\Pi})_\perp\rangle + \langle(R^2\nabla\phi\cdot\nabla\cdot\overleftrightarrow{\Pi})_{\mathrm{gv}}\rangle \approx \langle(R^2\nabla\phi\cdot\nabla\cdot\overleftrightarrow{\Pi})_{\mathrm{gv}}\rangle = -\left\langle\frac{1}{Rh_\theta h_r}\frac{\partial}{\partial r}\left[R^3\eta_4\frac{\partial(V_\phi R^{-1})}{\partial\theta}\right]\right\rangle = R_0\overline{n}_j m_j\nu_{\mathrm{d}j}\overline{V}_{\phi j}, \quad (32)$$

where $\eta_{4j} = n_j m_j T_j/e_j B$, the gyroviscous transport (or 'drag') frequency is given by

$$\nu_{\mathrm{d}j} \approx \nu_{\mathrm{d}j}^1 + \nu_{\mathrm{d}j}^2 \quad (33)$$

with

$$\nu_{\mathrm{d}j}^{1} = -\frac{T_j}{R_0 e_j \overline{B}_\phi}\varepsilon \left[\begin{array}{l} \widetilde{V}_{\phi j}^{\mathrm{s}}\left(2\left\langle \cos\theta \dfrac{\cos\xi}{h_\theta h_r}\right\rangle \right. \\ \quad + \dfrac{1}{R_0}\left\langle R\cos\theta \dfrac{\cos\xi}{h_\theta h_r}\right\rangle \\ \quad + \dfrac{1}{R_0}\left\langle R\sin\theta \dfrac{\sin\xi}{h_\theta h_r}\right\rangle \\ \quad + \dfrac{1}{R_0}x\left\langle R\sin\theta\cos\theta \dfrac{\sin\xi}{h_\theta h_r}\right\rangle\Big) \\ \quad + \widetilde{n}_j^{\mathrm{s}} \dfrac{1}{R_0}\left(\left\langle R\sin\theta \dfrac{\sin\xi}{h_\theta h_r}\right\rangle \right. \\ \quad + x\left\langle R\sin\theta\cos\theta \dfrac{\sin\xi}{h_\theta h_r}\right\rangle\Big), \end{array}\right], \quad (34)$$

$$\nu_{\mathrm{d}j}^{2} \equiv \frac{1}{2}\frac{\widetilde{\theta}_j G_j T_j}{R_0^2 e_j \bar{B}_\phi}, \quad (35)$$

where

$$G_j \equiv r(L_{\overline{n}_j}^{-1} + L_{T_j}^{-1} + L_{\overline{V}_{\phi j}}^{-1}), \quad (36)$$

$$\widetilde{\theta}_j = 2\varepsilon \left[\begin{array}{l} \widetilde{V}_{\phi j}^{\mathrm{s}}\left(\widetilde{n}_j^{\mathrm{c}}\left\langle R\dfrac{\cos^2\theta}{h_\theta h_r}\right\rangle + \dfrac{1}{\varepsilon}\left\langle R\dfrac{\cos\theta}{h_\theta h_r}\right\rangle \right. \\ \quad + \left\langle R\cos\theta\dfrac{\cos\xi}{h_\theta h_r}\right\rangle + \left\langle R\sin\theta\dfrac{\sin\xi}{h_\theta h_r}\right\rangle \\ \quad + x\left\langle R\sin\theta\cos\theta\dfrac{\sin\xi}{h_\theta h_r}\right\rangle\Big) \\ \quad + \widetilde{n}_j^{\mathrm{s}}\Big(- \widetilde{V}_{\phi j}^{\mathrm{c}}\left\langle R\dfrac{\sin^2\theta}{h_\theta h_r}\right\rangle + \left\langle R\sin\theta\dfrac{\sin\xi}{h_\theta h_r}\right\rangle \\ \quad + x\left\langle R\sin\theta\cos\theta\dfrac{\sin\xi}{h_\theta h_r}\right\rangle\Big) \end{array}\right]. \quad (37)$$

We note that there is mention in the literature of a 'gyroviscous cancellation' of inertial and gyroviscous terms, e.g. as discussed in [28]. One of many terms in the gyroviscous representation of that paper has a $(u^* \cdot \nabla)u$ form that is formally similar to the $(u \cdot \nabla)u$ inertial term (although u^* is a magnetization velocity whereas u is the fluid mass velocity). These two terms may add or subtract, depending on the signs of these velocities (directions of currents and magnetic fields), and the terminology 'gyroviscous cancellation' is rather misleading for this reason as well as because of the existence of the other gyroviscous terms. In this paper the magnitudes of the gyroviscous and inertial terms are primarily determined by the poloidal asymmetries, which are calculated from momentum balance in the elongated Miller model flux surface geometry; if the poloidal asymmetries vanished or were assumed to vanish, then the gyroviscosity would vanish. Neither a specific flux surface geometry nor the representation of poloidal asymmetries were considered in [28], so it is not really possible to further compare the present results with those of that paper.

Earlier circular model studies [12, 30–33] were done with $\nu_{\mathrm{d}j}^2$ only, but $\nu_{\mathrm{d}j}^1$ was identified to have non-negligible contribution during the numerical calculation in this work, thus was included for both the Miller model and the revised circular model theories (see appendix B for the revised circular model formalism). $\nu_{\mathrm{d}j}^2$ contains the same G_j and $\widetilde{\theta}_j$ representing the radial gradients and poloidal asymmetries respectively, thus allowing direct comparison with the earlier circular model formalism [12, 30–33]. Note here in equation (32) that the gyroviscous contribution accounts for the most of the viscous torque since it is much larger than the perpendicular component by the following argument. Braginskii's parallel (η_0), gyroviscous ($\eta_{3,4}$), and perpendicular ($\eta_{1,2}$) viscosity coefficients in a collisional plasma are given as follows, expressed with their relative orderings:

$$\eta_0 = 0.96 n T \tau, \qquad \eta_1 = \frac{3}{10}\frac{nT}{\Omega^2\tau},$$
$$\eta_2 = 4\eta_1, \qquad \eta_3 = \frac{1}{2}\frac{nT}{\Omega}, \qquad \eta_4 = 2\eta_3, \quad (38)$$

where in tokamak plasmas $\tau \sim 10^{-5}$ s is the typical self-collision time and $\Omega \sim 10^8\,\mathrm{s}^{-1}$ is the typical ion gyrofrequency. Thus, Braginskii's parallel, gyroviscous, and perpendicular viscosity coefficients are in the ratio of $1/(\Omega\tau)^{-1}/(\Omega\tau)^{-2} \approx 1/10^{-3}/10^{-6}$. Therefore, the ordering among these components are given by $\eta_0 \gg \eta_4 \gg \eta_2$. With the parallel contribution identically vanishing in the FSA and $\eta_4 \approx (\Omega\tau)\eta_2 \approx (10^3\text{–}10^4)\eta_2$, the gyroviscous contribution to toroidal momentum transport is the dominant one, larger than the perpendicular component generally by a couple of orders of magnitude. Note that we will use a more sophisticated form of the parallel viscosity, equation (21), when calculating the poloidal velocity and momentum transport in the following section.

The gyroviscous momentum transport frequency given by equation (33) is a strong function of density and toroidal velocity asymmetries, thus vanishes in any formalism that neglects poloidal dependences. Also, although Braginskii's viscosity was derived assuming large collisionality, this PS type 'neoclassical' gyroviscosity is independent of any explicit collisionality since no direct evidence on the trapped particle effect on gyroviscosity has been reported. When the poloidal asymmetries are not considered, as in the NCLASS code [39], only the perpendicular contribution survives and the calculated neoclassical momentum damping is negligible [19, 20, 26], leading to the incorrect conclusion that neoclassical transport is too small.

3.2. Stacey–Sigmar poloidal rotation theory with the Miller model

Calculation of the toroidal angular torques and transport rates in the previous section requires a calculation of the poloidal asymmetries ($n_j^{\mathrm{c,s}}$ and $V_j^{\mathrm{c,s}}$) appearing in equations (22*a*) and (22*b*). This can be accomplished by taking Fourier moments (i.e. 1, cosine and sine moments) of the poloidal momentum balance, equation (19), with equations (22*a*) and (22*b*) assumed. Using the same Fourier moments of the continuity equation (13), the velocity asymmetries ($V_j^{\mathrm{c,s}}$) can be related to the density asymmetries ($n_j^{\mathrm{c,s}}$) by

$$\widetilde{V}_{\theta j}^{\mathrm{s}} \equiv V_{\theta j}^{\mathrm{s}}/\varepsilon \approx -\widetilde{n}_j^{\mathrm{s}}, \quad (39)$$

$$\widetilde{V}_{\theta j}^{\mathrm{c}} \equiv V_{\theta j}^{\mathrm{c}}/\varepsilon = -\widetilde{n}_j^{\mathrm{c}} + \frac{1}{\varepsilon}\left\langle \frac{1}{R}\frac{\partial R}{\partial\theta}\sin\theta\frac{1}{h_\theta}\right\rangle \Big/ \left\langle \sin^2\theta\frac{1}{h_\theta}\right\rangle \quad (40)$$

to reduce the number of unknowns in the final computation model. We may consider adding an additional atomic physics term on the right-hand side of the continuity equation, equation (9), to increase the accuracy in the plasma edge region

as in one of the early circular model studies [44] but this is left as a future research.

We also assume the same type of Fourier series expansion for the electrostatic potential,

$$\Phi(r,\theta) \approx \overline{\Phi}(r)[1 + \Phi^{\mathrm{c}}(r)\cos\theta + \Phi^{\mathrm{s}}(r)\sin\theta], \tag{41}$$

and use it in the moments of the poloidal momentum balance equation for 'j = electrons' to relate the potential asymmetries ($\Phi^{\mathrm{c/s}}$) to the electron density asymmetries ($n_{\mathrm{e}}^{\mathrm{c/s}}$). In doing so, we neglect all other terms except the pressure and electric field terms in the poloidal momentum balance, equation (19), to get

$$\overline{\Phi}\Phi^{\mathrm{c,s}} = T_{\mathrm{e}} n_{\mathrm{e}}^{\mathrm{c,s}}/e \tag{42}$$

where $n_{\mathrm{e}}^{\mathrm{c,s}}$ are related $n_j^{\mathrm{c,s}}(j = \text{ions})$ by charge neutrality ($n_{\mathrm{e}}^{\mathrm{c,s}} = \sum_j Z_j n_j^{\mathrm{c,s}}$), a consequence of the assumption of ambipolar electron transport. The same Fourier moments of the radial momentum balance, equation (14), can be used to calculate the radial electric field, $\overline{E}_r$, and the toroidal velocity asymmetries ($V_{\phi j}^{\mathrm{c/s}}$) as a function of $n_j^{\mathrm{c,s}}$ as follows, again allowing the reduction in the number of unknowns in the numerical computation model. The 1, cosine, and sine moments respectively of the reduced radial momentum balance, equation (14), are

$$\begin{aligned}\widehat{\Phi}_j' &\equiv \frac{\overline{\Phi}'}{V_{\mathrm{th}j}} \equiv \frac{1}{V_{\mathrm{th}j}\overline{B}_\theta}\frac{\partial\overline{\Phi}}{\partial r} = -\frac{\overline{E}_r}{V_{\mathrm{th}j}\overline{B}_\theta} \\ &= \widehat{V}_{\theta j}\frac{\left\langle\dfrac{1}{1+\varepsilon\cos\xi}\right\rangle}{\left\langle\dfrac{1}{h_r}\right\rangle} - \widehat{V}_{\phi j}\left(1 + \frac{\partial R_0(r)}{\partial r}\right) \\ &\times\frac{\left\langle\dfrac{1}{(1+\varepsilon\cos\xi)}\dfrac{1}{h_r}\right\rangle}{\left\langle\dfrac{1}{h_r}\right\rangle} - \widehat{P}_j',\end{aligned} \tag{43}$$

where

$$\begin{aligned}&\widehat{P}_j' \equiv \frac{\overline{p}_j'}{V_{thj}} \equiv \frac{1}{V_{\mathrm{th}j}}\frac{1}{\overline{n}_j e_j \overline{B}_\theta}\frac{\partial\overline{p}_j}{\partial r}, \quad f_p \equiv B_\theta/B_\phi, \\ &\widehat{V}_{\theta j} \equiv \overline{V}_{\theta j}/(f_p V_{\mathrm{th}j}) \quad \text{and} \quad \widehat{V}_{\phi j} \equiv \overline{V}_{\phi j}/V_{\mathrm{th}j},\end{aligned}$$

$$\widetilde{V}_{\phi j}^{s} = \widetilde{n}_j^{s}\alpha_j^{1S} + \alpha_j^{2S}, \tag{44}$$

where α_j^{1S} and α_j^{2S} can be found in appendix C.

$$\begin{aligned}\widetilde{V}_{\phi j}^{\mathrm{c}} = \frac{\widehat{V}_{\theta j}}{\widehat{V}_{\phi j}}&\left(\alpha_j^{3C} + \alpha_j^{2C}\frac{\left\langle\dfrac{1}{1+\varepsilon\cos\xi}\right\rangle}{\left\langle\dfrac{1}{h_r}\right\rangle}\right) + \alpha_j^{1C} \\ &-\alpha_j^{2C}\left(1 + \frac{\partial R_0(r)}{\partial r}\right)\frac{\left\langle\dfrac{1}{(1+\varepsilon\cos\xi)}\dfrac{1}{h_r}\right\rangle}{\left\langle\dfrac{1}{h_r}\right\rangle} \\ &-\frac{\widehat{P}_j'}{\widehat{V}_{\phi j}}(\alpha_j^{2C} - \alpha_j^{4C}),\end{aligned} \tag{45}$$

where α_j^{1C}, α_j^{2C}, α_j^{3C}, and α_j^{4C} are all functions of $\widetilde{n}_j^{\mathrm{c}}$ and can be found in appendix C.

Using all the coupling relations found so far, the first moment of the poloidal momentum balance reduces to equation (46), written in a generic form for simplicity, that allows us to calculate the poloidal velocity for two ion species 'j' and 'k':

$$A_{11}\widehat{V}_{\theta j}^2 + A_{12}\widehat{V}_{\theta j} + A_{13}\widehat{V}_{\theta k} = B_1, \tag{46}$$

where A_{11}, A_{12}, A_{13} and B_1 are given in appendix C. In this equation, the friction term appears in $\nu_{jk}^* = \nu_{jk}qR/V_{\mathrm{th}j}$ and the viscous term in $f_j = \varepsilon^{-3/2}\nu_{jj}^*/((1+\varepsilon^{-3/2}\nu_{jj}^*)(1+\nu_{jj}^*))$ from the use of neoclassical parallel viscosity expression, $\eta_{0j} = n_j m_j V_{\mathrm{th}j} q R f_j(\nu_{jj}^*)$.

The cosine and sine moments of the poloidal momentum balance, equation (19), reduce to equations (47) and (48), respectively (again in generic forms for the two species), to solve for $\widetilde{n}_j^{\mathrm{c,s}}$,

$$A_{C1}\widetilde{n}_j^{\mathrm{c}} + A_{C2}\widetilde{n}_j^{\mathrm{s}} + A_{C3}\widetilde{n}_k^{\mathrm{c}} = B_C, \tag{47}$$

$$A_{S1}\widetilde{n}_j^{\mathrm{c}} + A_{S2}\widetilde{n}_j^{\mathrm{s}} + A_{S3}\widetilde{n}_k^{\mathrm{s}} = B_S, \tag{48}$$

where $A_{C,S}$ and $B_{C,S}$ coefficients are given in appendix C. When we assume 'two-species' plasma with the main ion (deuterium) and a majority impurity (carbon), equations (46)–(48) provide six equations, with j being either deuterium or carbon and k being the other, leaving two more relations to be identified from the toroidal angular momentum balance for the calculation of toroidal velocities.

3.3. Toroidal rotation calculation model with the Miller geometry

The calculation model for the toroidal velocity can be derived from the toroidal component of the angular momentum balance,

$$\begin{aligned}n_j m_j[R(\vec{V}_j\cdot\nabla)\vec{V}_j]_\phi + [R(\nabla\cdot\overleftrightarrow{\mathbf{\Pi}}_j)]_\phi &= Rn_j e_j E_\phi^A \\ +Rn_j e_j V_{rj}B_\theta + RF_{\phi j} + RM_{\phi j} - Rn_j m_j \nu_{\mathrm{atom}\,j} V_{\phi j},&\end{aligned} \tag{49}$$

from which we can get two additional relations to complete the eight equations to solve for the eight unknowns (four velocities and four density asymmetries). Using the FSAs of the first (inertial) and second (viscous) torque terms presented in equations (30) and (32), we can take FSAs of all other terms in equation (19) to find relations for the toroidal velocity calculation. The first moment of equation (49) yields

$$\begin{aligned}\overline{n}_j m_j \sum_k \overline{\nu}_{jk}[(1+\beta_j)\overline{V}_{\phi j} - \overline{V}_{\phi k}] &\equiv \overline{n}_j m_j \sum_k \overline{\nu}_{jk} y_j \\ = \overline{n}_j e_j E_\phi^A + \left(1 + \frac{\partial R_0(r)}{\partial r}\right)&\left\langle\frac{1}{h_r}\right\rangle e_j \overline{B}_\theta \Gamma_{rj} + \overline{M}_{\phi j},\end{aligned} \tag{50}$$

where $\beta_j \equiv (\nu_{\mathrm{d}j} + \nu_{nj} + S_{\mathrm{nb}j}/\overline{n}_j)/\overline{\nu}_{jk}$, $y_j \equiv (1+\beta_j)\overline{V}_{\phi j} - \overline{V}_{\phi k}$, and $\overline{M}_\phi$ is the toroidal momentum input. β_j represents the radial transport of angular momentum with $S_{\mathrm{nb}j}$ being the local neutral beam source rate and ν_{nj} and $\nu_{\mathrm{d}j}$ are the inertial and gyroviscous transport frequencies respectively calculated with equation (31) and (33). Thus, a relation between the toroidal velocities of deuterium and impurity can be derived by adding y_j of the two species, $j = i$ (deuterium) and $j = I$ (carbon) with $V_{\mathrm{th}i} = \sqrt{m_I/m_i}V_{\mathrm{th}I}$ when assuming equilibrium temperature ($T_i = T_I$). This yields

$$\widehat{V}_{\phi i}\sqrt{m_I/m_i}\beta_i + \widehat{V}_{\phi I}\beta_I = (y_i + y_I)/V_{\mathrm{th}I}, \tag{51}$$

which becomes the seventh equation in the numerical computation model. The last equation comes from manipulating the first moments of radial momentum balance, equation (43), for the two species. Since $\overline{\Phi}' \equiv 1/\overline{B}_\theta \partial\overline{\Phi}/\partial r$ is independent of species, it must be identical when calculated with either $j = i$ or $j = I$, thus providing

$$\widehat{V}_{\phi i} - \sqrt{\frac{m_i}{m_I}}\widehat{V}_{\phi I} = \left(\widehat{V}_{\theta i} - \sqrt{\frac{m_i}{m_I}}\widehat{V}_{\theta I}\right) \times \frac{\left\langle \dfrac{1}{1+\varepsilon\cos\xi}\right\rangle}{\left(1+\dfrac{\partial R_0(r)}{\partial r}\right)\left\langle \dfrac{1}{(1+\varepsilon\cos\xi)}\dfrac{1}{h_r}\right\rangle} + \left(-\widehat{P}_i' + \sqrt{\frac{m_i}{m_I}}\widehat{P}_I'\right) \times \frac{\left\langle \dfrac{1}{h_r}\right\rangle}{\left(1+\dfrac{\partial R_0(r)}{\partial r}\right)\left\langle \dfrac{1}{(1+\varepsilon\cos\xi)}\dfrac{1}{h_r}\right\rangle}, \tag{52}$$

which is the last eighth relation that the toroidal velocities of both species must satisfy.

We have not considered electrons in the above formalism under the assumption that ion-impurity collision frequencies are much greater than ion-electron collision frequencies, which is the case in most tokamak experiments. We implicitly treat electrons by assuming that the resulting theory is ambipolar.

4. Numerical computation model

Six equations from the extended S–S poloidal rotation model plus two equations from the toroidal rotation calculation model from the previous section constitute a self-consistent set of eight equations that we designate extended neoclassical rotation theory. These equation may be solved for the toroidal and poloidal velocities and the sin and cos density asymmetries for the two species, at each radial mesh point from the centre of plasma to the edge (we use 51 mesh points). Note that all the unknowns in the calculation model are normalized values so that numerical round-off errors are minimized:

$$\begin{aligned}
&\widehat{V}_{\phi i} = \widehat{V}_{\phi \mathrm{D}} = \widehat{V}_{\mathrm{tD}} : \text{Toroidal velocity (deuterium)}\\
&\quad \widetilde{n}^{\mathrm{c}}_{\mathrm{D}} = \widetilde{n}^{\mathrm{c}}_i : \text{Cos asymmetry (deuterium)},\\
&\widehat{V}_{\phi I} = \widehat{V}_{\phi \mathrm{C}} = \widehat{V}_{\mathrm{tC}} : \text{Toroidal velocity (carbon)}\\
&\quad \widetilde{n}^{\mathrm{c}}_{\mathrm{C}} = \widetilde{n}^{\mathrm{c}}_I : \text{Cos asymmetry (carbon)},\\
&\widehat{V}_{\theta i} = \widehat{V}_{\theta \mathrm{D}} = \widehat{V}_{\mathrm{pD}} : \text{Poloidal velocity (deuterium)}\\
&\quad \widetilde{n}^{\mathrm{s}}_{\mathrm{D}} = \widetilde{n}^{\mathrm{s}}_i : \text{Sin asymmetry (deuterium)},\\
&\widehat{V}_{\theta I} = \widehat{V}_{\theta \mathrm{C}} = \widehat{V}_{\mathrm{pC}} : \text{Poloidal velocity (carbon)}\\
&\quad \widetilde{n}^{\mathrm{s}}_{\mathrm{C}} = \widetilde{n}^{\mathrm{s}}_I : \text{Sin asymmetry (carbon)}.
\end{aligned} \tag{53}$$

A numerical algorithm is designed to solve the non-linearly coupled set of eight equations iteratively, using the decomposition given in equations (54*a*)–(54*c*), written in generic forms:

$$\begin{bmatrix} c_{11} & c_{12} \\ c_{21} & c_{22} \end{bmatrix}\begin{bmatrix} \widehat{V}_{\theta i} \\ \widehat{V}_{\theta I} \end{bmatrix} = \begin{bmatrix} d_1 \\ d_2 \end{bmatrix}, \tag{54a}$$

$$\begin{bmatrix} a_{11} & a_{12} & a_{13} & 0 \\ a_{21} & a_{22} & 0 & a_{24} \\ a_{31} & 0 & a_{33} & a_{34} \\ 0 & a_{42} & a_{43} & a_{44} \end{bmatrix}\begin{bmatrix} \widetilde{n}^{\mathrm{c}}_i \\ \widetilde{n}^{\mathrm{s}}_i \\ \widetilde{n}^{\mathrm{c}}_I \\ \widetilde{n}^{\mathrm{s}}_I \end{bmatrix} = \begin{bmatrix} b_1 \\ b_2 \\ b_3 \\ b_4 \end{bmatrix}, \tag{54b}$$

$$\begin{bmatrix} e_{11} & e_{12} \\ e_{21} & e_{22} \end{bmatrix}\begin{bmatrix} \widehat{V}_{\phi i} \\ \widehat{V}_{\phi I} \end{bmatrix} = \begin{bmatrix} f_1 \\ f_2 \end{bmatrix}. \tag{54c}$$

This decomposition proved to be better-conditioned and more iteratively stable than the entire set of eight-by-eight non-linear systems taken as a single set since the latter was shown to be extremely ill-conditioned. To iteratively solve this non-linear system of equations for comparison with experiment, the initial guesses for carbon velocities are taken directly from the experimental measurements, and for deuterium velocities perturbation theory [45] is used to infer initial guesses from carbon velocity measurements. Initial density asymmetries are set to zeros and subsequent values are generated as iterations continue. The numerical algorithm for this Miller model study can be best described as a combination of successive over relaxation (SOR) and simulated annealing (SA) and is developed independently from the earlier circular model calculation algorithm [30] but shares very similar numerical characteristics. More detailed description of this numerical algorithm will be presented in a separate publication along with all the coefficients.

In earlier studies with the circular model [30, 45], the Shafranov shift was not considered for simplicity but is represented in this study with the following form of the analytic Shafranov shift model [34],

$$\frac{\partial R_0}{\partial r} = \Delta' \equiv -(r/R_0)\left(\beta_\theta + \frac{1}{2}\ell_{\mathrm{i}}\right), \tag{55}$$

where $\beta_\theta = nT/(B_\theta^2/2\mu_0)$ and ℓ_{i} is the internal inductance. Study with more accurate Shafranov shift models can be done when these are considered to be critical for accuracy.

5. Experimental data

Since the new rotation theory was developed based on Braginskii's strong rotation orderings, two strongly rotating ELMing (edge-localized mode) H-mode DIII-D shots are analysed in this paper. One shot was counter-injection #138639 (2085 ms) and the other was co-injection #142020 (2310 ms). The main toroidal rotation drive for both shots was provided by directed neutral beam injection. A summary of the shot parameters is provided in table 1. In this table, the impurity/deuterium density ratio shows the relative amount of impurities with respect to deuterium density. For example, shot 138639 has approximately 10% impurities on average with ∼9% at the centre and ∼10% at the 90% flux surfaces. Throughout the radial ranges except the plasma edge, the ratio only slightly fluctuates about the average but the fluctuation increases at more than 90% flux surfaces where the ratio is not reliable due to lack of atomic physics treatment on the edge. The incident neutral beam power (P_{NB}) is given as the ratio of incident vs. capable neutral beam power, which is identical to the duty cycle. For example, the 30LT beam for shot 142020 (1.3 MW/2.6 MW) has the capability of 2.6 MW beam injection but used with 50% duty cycle, thus generating 1.3 MW of beam injection energy. Figure 2 shows the equilibrium flux surfaces for the two shots.

We note that there have been recent advances in the measurements and analysis of toroidal and poloidal rotation, including proper treatment of the apparent velocity caused

Table 1. Summary of two DIII-D shot parameters.

Shot properties	Shot 138639(2085 ms)	Shot 142020(2310 ms)
Beam injection direction	Counter-injection	Co-injection
R (major radius)	1.734 m	1.796 m
a (minor radius)	0.586 m	0.592 m
$\kappa(r=0)/\kappa(r=a)$ (elongation)	1.45/1.83	1.39/1.85
$\delta(z_{\text{bottom}})/\delta(z_{\text{top}})$ (triangularity)	0.22/0.6	0.714/0.382
I (current)	−1.181 MW (CW from the top view)	1.074 MW (CCW from the top view)
B_{p} (poloidal magnetic strength)	0.275 T	0.249 T
B_{ϕ} (toroidal magnetic strength)	−1.994 T	−1.897 T
q_{95}(safety factor at 95% flux surface)	4.9	5.63
V_{loop} (loop voltage)	−0.262 96 V	0.315 715 V
Divertor configuration	Upper single null (USN)	Lower single null (LSN)
Impurity/deuterium density ratio (average/at the centre/at 95% flux surfaces)	0.1/0.09/0.1	0.04/0.04/0.05
P_{NB} (incident power/capable power)	30LT (2.1/2.6 MW), 150LT (2.2/2.2 MW), 330LT (2.6/2.6 MW)	30LT (1.3 MW/2.6 MW), 150LT (1.8 MW/1.8 MW), 330LT (1.1 MW/2.2 MW), 330RT (1.3 MW/2.2 MW)

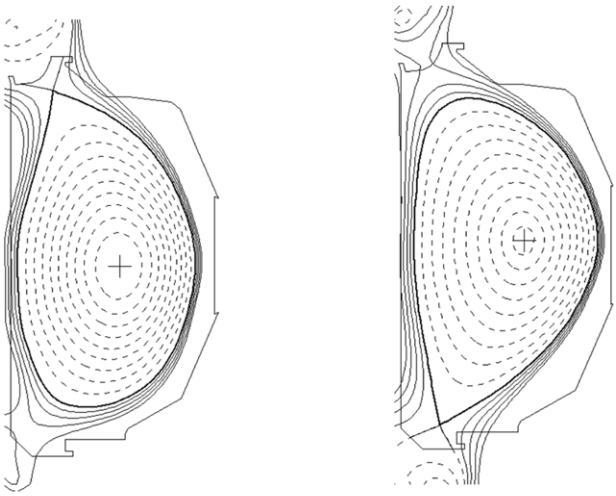

Figure 2. Equilibrium flux surfaces of two DIII-D shots.

by the energy dependent cross-section [46–48], as well as extensions to the circular model theory since the earlier comparison [30]. Comparison of the calculated velocities from the new plasma rotation theory against these measurements are presented in the following section. Although only two shots were analysed in this study, a good combination of co- and counter-injection, different directions of B_{θ} and I_{p}, and the different extent of poloidal dependences of upper and lower divertors (as will be shown in the next section) enables a good test of the theory and the numerical algorithm. Efforts to identify more suitable shots are underway, especially shots which take advantage of the recent advances in the measurement of deuterium velocity and analysis [49].

6. Comparison of theory with experiment

Figures 3 and 4 show the calculated rotation velocities compared to the experimental measurement for both shots. For all the figures in this paper, 't' represents 'toroidal', 'p' for 'poloidal', 'D' or 'i' for deuterium, and 'C' or 'I' for carbon. In these figures Vt_D^{computed} and Vp_D^{computed} (blue diamonds) are the calculated, thus predicted, toroidal and poloidal deuterium velocities respectively for which no measurements are available. $\rho = r/a$ on the x-axis is the normalized distance from the centre of plasma to the flux surface. Overall, these two sets of the calculated results show that the new neoclassical plasma rotation theory based on the Miller equilibrium flux surface geometry predicts carbon toroidal and poloidal rotation velocities which agree quite well with measured values, generally to within approximately <10%. The notable exception of a significant under-prediction of the poloidal velocity in the edge region of the co-injected shot #142020 is probably attributable to not taking into account charge-exchange damping, the effect of divertor on poloidal asymmetry in the prediction, use of Braginskii's strong rotation ordering in the edge where rotation is much weaker, and ill-conditioning of the numerical calculation model in the edge. Overall this is a significant improvement relative to the earlier studies with the circular model [30], in which the measured carbon toroidal velocities were overpredicted by roughly a factor of 2 and the disagreement in predicted and measured carbon poloidal velocities was much larger.

Figure 5 shows the calculated density asymmetries ($n_{i,I}^{\text{c,s}}$), which are relatively small (less than 10% everywhere except in the very edge). These asymmetries are larger for carbon than for deuterium. Note that a positive/negative sine component indicates an upward/downward asymmetry in the density distribution, while a positive/negative cosine component indicates an outward/inward asymmetry in the density distribution. The velocity asymmetries ($V_{i,I}^{\text{c,s}}$) are coupled with $n_{i,I}^{\text{c,s}}$ by equations (39), (40), (44) and (45), thus can be easily computed from these density asymmetries.

The inertial and gyroviscous toroidal angular momentum transport frequencies are strong functions of poloidal asymmetries as shown in equation (31) and (33)–(37). These transport frequencies are calculated with the density asymmetries shown in figure 5 and plotted in figures 6 and 7 for the range in which neglected edge phenomena are unimportant. Since the gyroviscous transport frequency is generally much larger than the inertial transport frequency and the deuterium density is much larger than the carbon density, the total toroidal

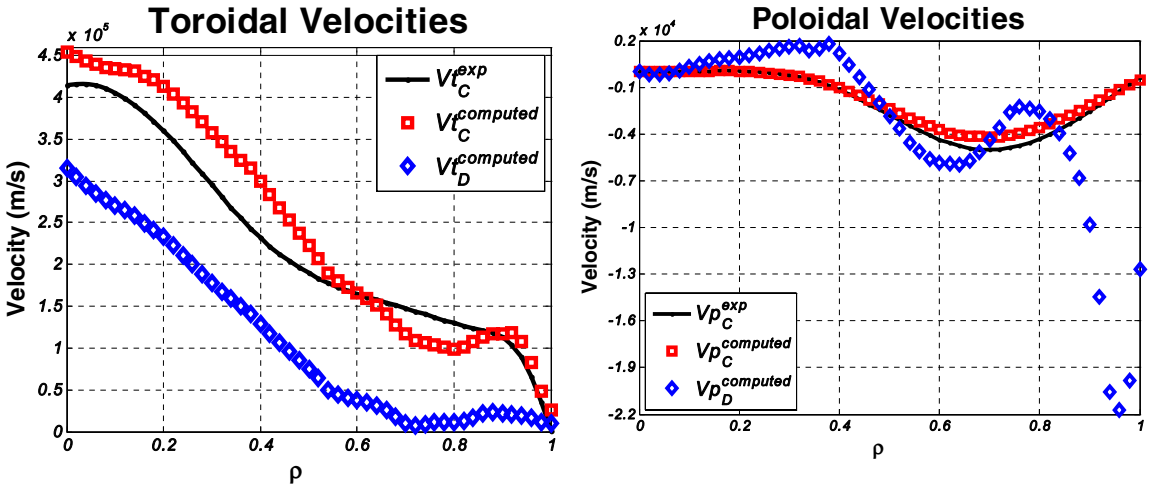

(a) $\overline{V}_\phi$ (CCW positive) (b) $\overline{V}_\theta$ (positive upward at outer mid-plane)

Figure 3. Calculated velocities for carbon and deuterium for counter-injected upper SN shot #138639.

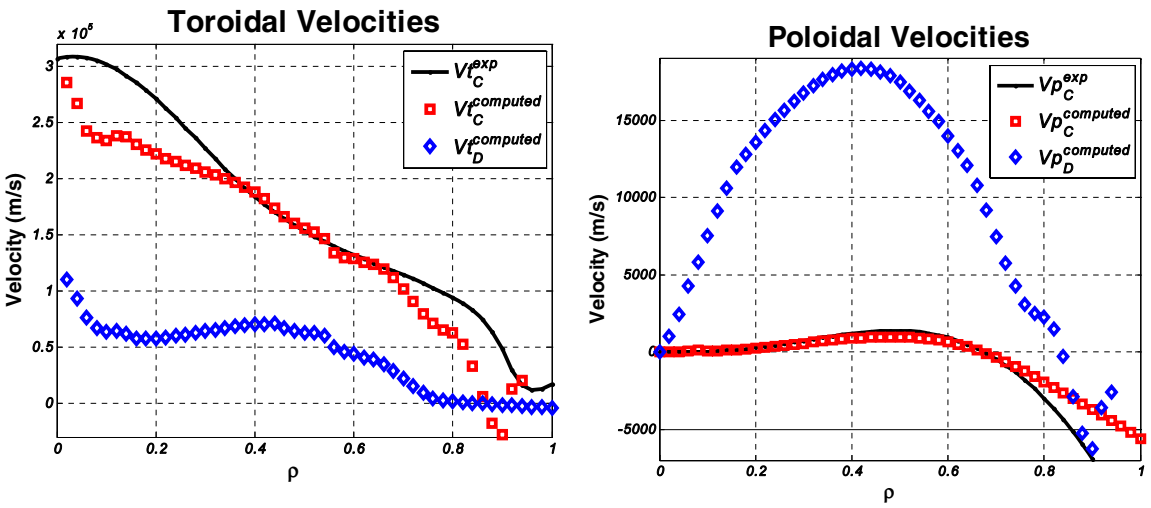

(a) $\overline{V}_\phi$ (CCW positive) (b) $\overline{V}_\theta$ (positive downward at outer mid-plane)

Figure 4. Calculated velocities for carbon and deuterium for co-injected lower SN shot 142020.

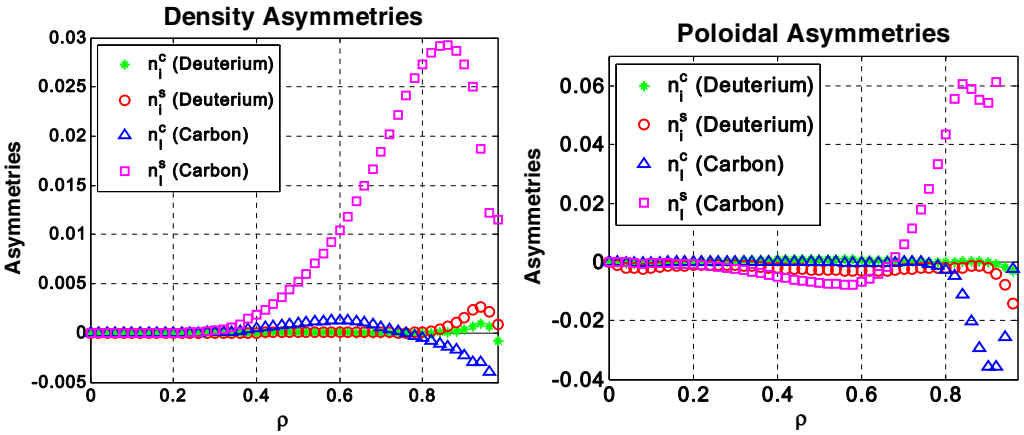

(a) Ctr-injection shot 138639 (b) Co-injected shot 142020

Figure 5. Density asymmetries for carbon and deuterium.

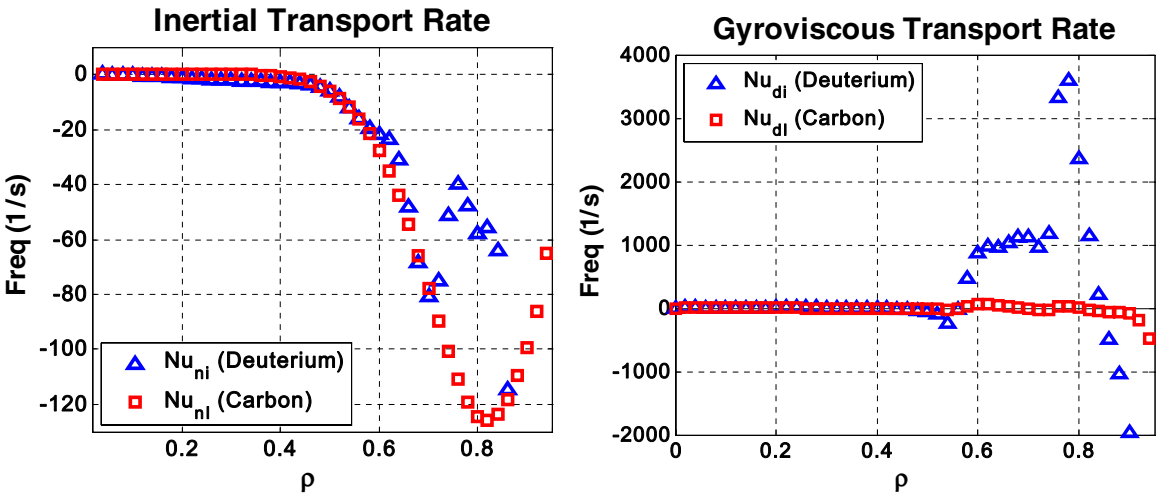

(a) Inertial transport frequency (b) Gyroviscous transport frequency

Figure 6. Toroidal angular momentum transport frequencies for counter-injected shot #138639.

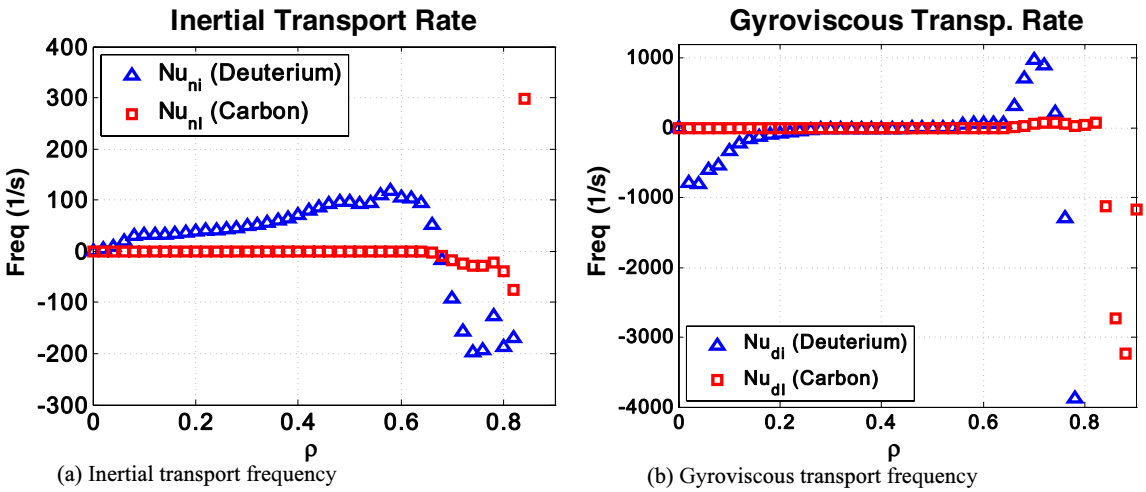

(a) Inertial transport frequency (b) Gyroviscous transport frequency

Figure 7. Toroidal angular momentum transport frequencies for co-injected shot #142020.

angular momentum transport frequency (neglecting charge-exchange) is essentially the gyroviscous toroidal angular momentum transfer frequency of deuterium, i.e. $\nu_j \approx \nu_{dj}$ where ν_j is the total transport rate of species j. Note that this significant neoclassical gyroviscous transport would vanish in a poloidal rotation theory that does not account for density and velocity asymmetries. It is notable that figures 6 and 7 imply both inward ($\nu_{nj}, \nu_{\mathrm{d}j} < 0$) and outward ($\nu_{nj}, \nu_{\mathrm{d}j} > 0$) angular momentum transport for both deuterium and carbon. Although the larger transfer frequencies in the plasma edge may be due in part to the $V_{\phi j} \sim V_{\mathrm{th}j}$ ordering of the Braginskii formalism and the neglect of charge-exchange, the profiles clearly imply both inward and outward momentum transport.

Since the circular model is just a special case of the Miller geometry (i.e. $\kappa = 1$ and $\delta = 0$ with no Shafranov shift), the same numerical algorithm can be used to calculate the velocities for the circular model theory. The predictions of the circular and Miller model theories are compared with the measured carbon velocities in figures 8 and 9. The Miller model predictions are in significantly better agreement with experiment than are the circular model predictions, due to the better representation of the poloidal dependence of the flux surfaces, which leads to a more accurate calculation of poloidal asymmetries and poloidal rotation velocities.

7. Relation to other work on neoclassical viscosity

The literature related to neoclassical viscosity is somewhat confusing. There are at least two versions of gyroviscosity in the literature, originating from the work of Braginskii [14] and from the work of Mikhailovskii and Tsypin [17], respectively, and there are other developments of viscosity (e.g. [19, 20]) that do not include gyroviscosity at all. In this section we briefly outline the relation of the gyroviscosity of this paper to the literature on neoclassical viscosity.

Most developments of viscosity for tokamak plasmas are based, directly or indirectly, on the methods of Chapman and Enskog [50]. Braginskii [14] was among the first to develop a model for viscosity in a plasma by partitioning the viscous stress tensor (in x–y–z geometry) into three components—parallel, perpendicular and gyro viscosity, with viscosity coefficients that differed by orders of magnitude

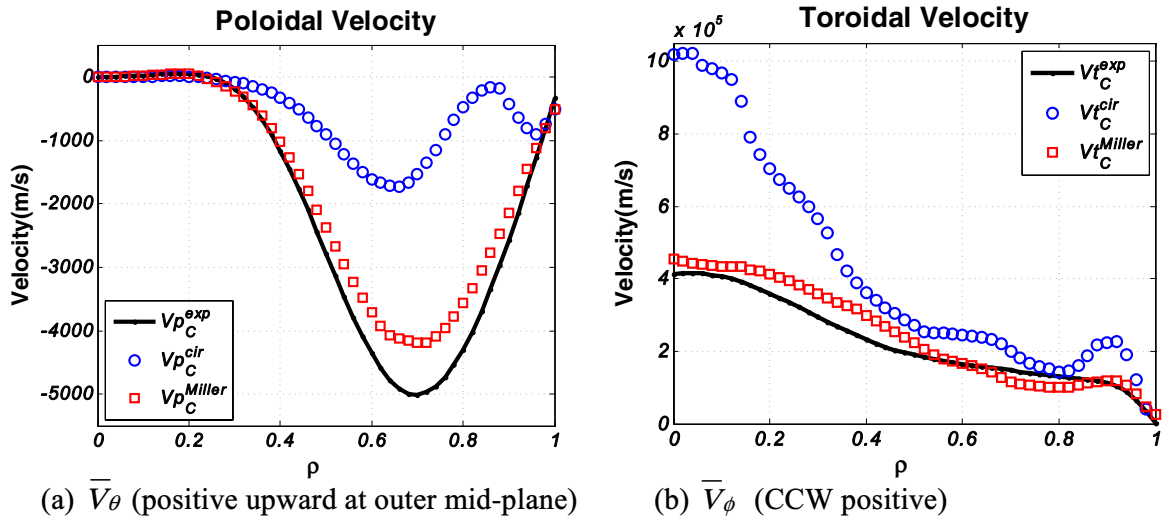

(a) $\overline{V}_\theta$ (positive upward at outer mid-plane) (b) $\overline{V}_\phi$ (CCW positive)

Figure 8. Comparison of predicted carbon velocities with the circular and Miller models with measurements for ctr-injected shot 138639.

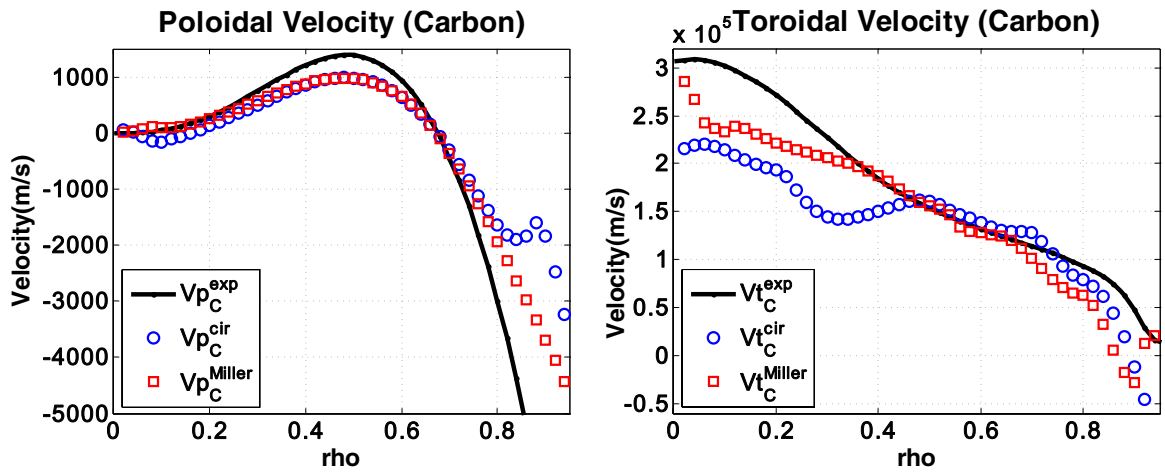

(a) $\overline{V}_\theta$ (positive downward at outer mid-plane) (b) $\overline{V}_\phi$ (CCW positive)

Figure 9. Comparison of predicted carbon velocities with the circular and Miller models with measurements for co-injected shot 142020.

($\eta_\parallel \gg \eta_\Omega \gg \eta_\perp$). The flux surface average of the parallel viscous force vanishes identically in toroidal flux surface geometry (so it does not contribute to toroidal momentum damping), and the perpendicular viscous force was found to be much too small to explain the toroidal angular momentum damping rate observed in tokamaks, leading to the (premature) conclusion that neoclassical viscosity could not account for observed toroidal momentum damping in tokamaks.

Stacey and Sigmar [18] extended the Braginskii formalism to toroidal flux surface geometry and showed that small up–down poloidal asymmetries in density, such as those measured for impurity ions in several tokamaks, could produce gyroviscous momentum damping rates comparable to those observed in tokamaks. Stacey [21] subsequently calculated (by solving the low order Fourier moments of the poloidal momentum balance equation numerically) the density asymmetries in several tokamaks and evaluated the resulting gyroviscous momentum damping rates that agreed reasonably well with observed damping rates. Similar calculations, based on a simple 'circular' model for the poloidal dependence of the flux surface geometry, were later made for several DIII-D discharges with widely different plasma parameters, with the general result that the measured momentum damping rates were under-predicted by only about a factor of two by the gyroviscous theory. This result motivated the work reported in this paper in which the poloidal dependence in the gyroviscous theory is represented by the more realistic Miller model [34] and the agreement between prediction and measurement is generally to within 10%.

Shortly after Braginskii's original paper, Mikhailovskii and Tsypin [17] noted that the strong rotation ordering used by Braginskii was inappropriate for tokamaks of that day (but not those of today) in which the rotation velocity was well below the thermal velocity, and these authors developed an alternative formalism in a weak rotation ordering. This line of theoretical development has been extended by several authors including Catto and Simikov [27, 29] and Ramos [28]. This development also yields a gyroviscous tensor similar to that obtained by Braginskii plus an additional gyroviscous tensor proportional to the thermal flux.

Over this same timeframe there were several other derivations of neoclassical viscosity (e.g. the work of Hinton and Wong [19] and of Conner, Cowley, Hastie and Pan [20]) that did not have a gyroviscous contribution. However, this work was based on a gyroradius ordering scheme which only retained leading (zero) order terms in the gyroradius parameter, and the poloidal asymmetries (and the poloidal velocity) enter these schemes at first order. Estimates of these first order terms made for some DIII-D discharges were comparable to values calculated numerically and observed experimentally [30], so such ordering schemes would also find gyroviscous contributions when carried to higher (first) order, as is necessary in order to touch base with experiment.

8. Conclusions

An extended neoclassical rotation and momentum plasma transport theory based on the Stacey–Sigmar model with the more accurate Miller equilibrium flux surface geometry was presented in this paper. It was also shown that the gyroviscous contribution to viscous transport, $(R^2\nabla\phi\cdot\nabla\cdot\overleftrightarrow{\mathbf{\Pi}})_{\rm gv}$, accounts for most of the neoclassical toroidal angular momentum damping in this model. Comparisons of the predictions of this new theory with experiment for two DIII-D discharges indicate that the new theory of this paper predicts the measured carbon poloidal and toroidal rotation very well ($<10\%$) everywhere except in the very edge, for the co-injected shot, where the neglect of recycling neutrals and of the divertor and the assumption of strong rotation ordering may be expected to cause difficulty. It is shown that the more accurate poloidal representation of the flux surfaces provided by the Miller equilibrium model is responsible for a significantly more accurate prediction than is possible with the similar neoclassical rotation theory based on the circular model [30].

The good agreement of prediction with experiment found on the two shots examined in this paper leads us to tentatively conclude that the extended neoclassical theory, when all important terms are retained and properly evaluated, is capable of accounting for most of the rotation and momentum transport in tokamaks. Such a conclusion must, of course, be confirmed by a more extensive comparison of prediction with experiment. Also, improved accuracy in the plasma edge requires extending the model further to represent charge-exchange of recycling neutrals, the effect of the divertor on poloidal asymmetries, and the weak rotation ordering of Mikhailovskii.

9. Future work

The derivations of this paper have been carried out in toroidal geometry with the primary intention of utilizing the Miller model to provide a better representation of poloidal asymmetries in the flux surface geometry, while retaining a tractable calculation model for toroidal rotation that could be compared with experimental results, in order to further the evaluation of the ability of a neoclassical gyroviscosity model to represent the radial transport of toroidal momentum in tokamak experiments. A necessary secondary purpose was to further develop a self-consistent model for the calculation of poloidal rotation and poloidal density asymmetries. While the comparisons with experiments are quite encouraging, there remain many minor and major refinements that could be made to the present calculation model.

The extended neoclassical rotation theory in this research is based on Braginskii's strong rotation ordering, $V_{\phi j}\simeq V_{{\rm th}j}$ and does not include neutral recycling and the associated atomic physics in the edge. It is straightforward to extend the continuity equation to include all the atomic physics effects and to include a neutral recycling calculation, as was done in one of the previous circular model studies [45].

Developing a weak rotation theory based on Mikhailovskii's weak rotation ordering, $V_{\phi j}\ll V_{{\rm th}j}$, would extend the applicability of the plasma rotation theory based on the model of this paper to a wider range of weaker plasma rotation, such as might be found in the plasma edge and in future larger tokamaks. Mikhailovskii's viscosity formalism [17] has been revised by other researchers and most recently by Catto and Simakov [27, 29] and Ramos [28]. A simple way of presenting Catto and Simakov's viscosity formalism to show its relation to Braginskii's is

$$\overleftrightarrow{\mathbf{\Pi}}_j^{\rm Mikhailovskii}=\overleftrightarrow{\mathbf{\Pi}}_j^{\rm Braginskii}+\overleftrightarrow{\mathbf{\Pi}}_j^{\rm Heat}, \tag{56}$$

which indicates that the current rotation theory can be modified by adding $\overleftrightarrow{\mathbf{\Pi}}_j^{\rm Heat}$ to the formalism, thus making the current theory a special case of the more general theory based on Mikhailovskii's ordering. In doing so, selectively adding some important terms with significant contribution from the heat equation terms may simplify the modification of the current theory and numerical algorithm. In this regard, use of Braginskii's formalism in this research can be considered as an intermediate step toward developing a more general neoclassical rotation theory for both strong and weak rotation orderings.

We have found that extension of the poloidal geometry representation from the simple 'circular' model [$R=R_0(1+r/R_0\cos\theta)$, $B=B_0/(1+r/R_0\cos\theta)$] to the Miller model resulted in significant improvement in the agreement between predicted and measured rotation velocities. However, even the Miller model does not represent up–down asymmetries in flux surface geometry nor the effect of divertors. Extension of the Miller flux surface geometry model to explicitly represent up–down asymmetries and the divertor should be possible.

In a similar vein, the representation of further poloidal asymmetries over the Miller model flux surfaces in flows and densities by a first-order Fourier series may not be capable of fully representing more extremely asymmetric distributions. If experimental or other evidence of the need for a more extreme asymmetric representation of the density flow arises in future applications, then there may be a need to extend the formalism to include a higher order Fourier representation of poloidal asymmetries in flow and density in future work.

In the longer term, it would be useful to repeat the derivations of this paper in more general representations, such as the coordinate-free representation of Ramos [28], and to investigate any effect on the resulting model of explicitly using the 'gyroviscous cancellation'.

Finally, we note that a rotation theory such as presented in this paper, which represents the effects of elongated and triangulated flux surface geometry and further takes into account poloidal variations of flows and densities over the flux surface, should enable an interesting study of the use of axisymmetric flux surface shaping to optimize flow properties, in particular after the representation is extended to incorporate vertical asymmetries and divertors.

Acknowledgments

The authors are grateful to the members of the DIII-D Team who made the measurements presented in this paper.

This work was supported by the US Department of Energy under grant DE-FG02-ER54538 with the Georgia Tech Research Corporation, contract DE-AC02-09CH11466 with the Princeton Plasma Physics Laboratory and contract DE-AC03-99ER54463 with General Atomics.

Appendix A. Inertial and viscosity terms in curvilinear geometry

(1) Inertial terms in curvilinear geometry:

$$[(\vec{V}\cdot\nabla)\vec{V}]_r = \frac{V_{rj}}{h_r}\frac{\partial V_{rj}}{\partial r} + \left[\frac{V_{\theta j}}{h_\theta}\frac{\partial V_{rj}}{\partial \theta} + \frac{V_{rj}V_{\theta j}}{h_r h_\theta}\left(\frac{\partial h_r}{\partial \theta} - \frac{\partial h_\theta}{\partial r}\right)\right] - \frac{V_{rj}V_{\phi j}}{h_r h_\phi}\frac{\partial h_\phi}{\partial r}, \tag{A1}$$

$$[(\vec{V}\cdot\nabla)\vec{V}]_\theta = \left[\frac{V_{rj}}{h_r}\frac{\partial V_{\theta j}}{\partial r} + \frac{V_{\theta j}V_{rj}}{h_\theta h_r}\left(\frac{\partial h_\theta}{\partial r} - \frac{\partial h_r}{\partial \theta}\right)\right] + \frac{V_{\theta j}}{h_\theta}\frac{\partial V_{\theta j}}{\partial \theta} - \frac{V_{\theta j}V_{\phi j}}{h_\theta h_\phi}\frac{\partial h_\phi}{\partial \theta}, \tag{A2}$$

$$[(\vec{V}\cdot\nabla)\vec{V}]_\phi = \left(\frac{V_{rj}}{h_r}\frac{\partial V_{\phi j}}{\partial r} + \frac{V_{\phi j}V_{rj}}{h_\phi h_r}\frac{\partial h_\phi}{\partial r}\right) + \left(\frac{V_{\theta j}}{h_\theta}\frac{\partial V_{\phi j}}{\partial \theta} + \frac{V_{\phi j}V_{\theta j}}{h_\phi h_\theta}\frac{\partial h_\phi}{\partial \theta}\right). \tag{A3}$$

(2) Viscosity terms in curvilinear geometry:

The rate-of-stress tensor elements in the viscous stress tensor is decomposed into

$$\Pi_{\alpha\beta} = \Pi^0_{\alpha\beta} + \Pi^{12}_{\alpha\beta} + \Pi^{34}_{\alpha\beta}, \tag{A4}$$

where

$$\Pi^0_{\alpha\beta} = -\eta_0 W^0_{\alpha\beta}, \qquad \Pi^{12}_{\alpha\beta} = -(\eta_1 W^1_{\alpha\beta} + \eta_2 W^2_{\alpha\beta}) \qquad \text{and} \qquad \Pi^{34}_{\alpha\beta} = \eta_3 W^3_{\alpha\beta} + \eta_4 W^4_{\alpha\beta}. \tag{A5}$$

The elements of the traceless rate-of-strain tensor are

$$\begin{aligned} W^0_{\alpha\beta} &\equiv \tfrac{3}{2}(f_\alpha f_\beta - \tfrac{1}{3}\delta_{\alpha\beta})(f_\mu f_\nu - \tfrac{1}{3}\delta_{\mu\nu})W_{\mu\nu}, \\ W^1_{\alpha\beta} &\equiv (\delta^\perp_{\alpha\mu}\delta^\perp_{\beta\nu} + \tfrac{1}{2}\delta^\perp_{\alpha\beta}f_\mu f_\nu)W_{\mu\nu}, \\ W^2_{\alpha\beta} &\equiv (\delta^\perp_{\alpha\mu}f_\beta f_\nu + \delta^\perp_{\beta\nu}f_\alpha f_\mu)W_{\mu\nu}, \\ W^3_{\alpha\beta} &\equiv \tfrac{1}{2}(\delta^\perp_{\alpha\mu}\varepsilon_{\beta\gamma\nu} + \delta^\perp_{\beta\nu}\varepsilon_{\alpha\gamma\mu})f_\gamma W_{\mu\nu}, \\ W^4_{\alpha\beta} &\equiv \tfrac{1}{2}(f_\alpha f_\mu\varepsilon_{\beta\gamma\nu} + f_\beta f_\nu\varepsilon_{\alpha\gamma\mu})f_\gamma W_{\mu\nu}, \end{aligned} \tag{A6}$$

where $\delta^\perp_{\alpha\beta} \equiv \delta_{\alpha\beta} - f_\alpha f_\beta$, $\delta_{\alpha\beta}$ the Kronecker delta function and $\varepsilon_{\alpha\beta\gamma}$ the antisymmetric unit tensor. The Einstein summation convention is also assumed. For tokamak plasmas, we can assume

$$f_r = |B_r|/|B| \approx 0, \qquad f_p = |B_\theta|/|B| \approx 0, \qquad f_\phi = |B_\phi|/|B| \approx 1. \tag{A7}$$

Neglecting V_r since $V_r \ll V_\theta < V_\phi \sim V_{\rm th}$, assuming axisymmetry ($\partial/\partial\phi \approx 0$), and with A_0 defined as

$$A_0 = -\frac{1}{3}(W_{rr} + W_{\theta\theta}) + \frac{2}{3}W_{\phi\phi} + 2f_p W_{\theta\phi} = 2\left[-\frac{1}{3h_\theta}\frac{\partial V_{\theta j}}{\partial\theta} + \left(\frac{1}{Rh_\theta}\frac{\partial R}{\partial\theta} + \frac{1}{3B_\theta h_\theta}\frac{\partial B_\theta}{\partial\theta}\right)V_{\theta j} + f_p R\frac{1}{h_\theta}\frac{\partial(V_{\phi j}R^{-1})}{\partial\theta}\right], \tag{A8}$$

the elements of the viscous stress tensors are given by

$$\Pi_{rr} = \frac{1}{2}\eta_0 A_0 + \eta_1\left[(RB_\theta)^{-1}\frac{1}{h_\theta}\frac{\partial(RB_\theta V_{\theta j})}{\partial\theta} - f_p\frac{R}{h_\theta}\frac{\partial(V_{\phi j}R^{-1})}{\partial\theta}\right] - \eta_3\left[\frac{h_\theta}{h_r}\frac{\partial(V_{\theta j}h_\theta^{-1})}{\partial r} - f_p\frac{R}{h_r}\frac{\partial(V_{\phi j}R^{-1})}{\partial r}\right], \tag{A9}$$

$$\Pi_{r\theta} = \Pi_{\theta r} = -\eta_1\frac{h_\theta}{h_r}\frac{\partial(V_{\theta j}h_\theta^{-1})}{\partial r} - (\eta_2 - \eta_1)f_p\frac{R}{h_r}\frac{\partial(V_{\phi j}R^{-1})}{\partial r} - \eta_3(RB_\theta)^{-1}\frac{1}{h_\theta}\frac{\partial(RB_\theta V_{\theta j})}{\partial\theta} - (\eta_4 - \eta_3)f_p\frac{R}{h_\theta}\frac{\partial(V_{\phi j}R^{-1})}{\partial\theta}, \tag{A10}$$

$$\Pi_{r\phi} = \Pi_{\phi r} = -\eta_2 R\frac{1}{h_r}\frac{\partial(V_{\phi j}R^{-1})}{\partial r} - \eta_4 R\frac{1}{h_\theta}\frac{\partial(V_{\phi j}R^{-1})}{\partial\theta}, \tag{A11}$$

$$\Pi_{\theta\theta} = \frac{1}{2}\eta_0 A_0 + \eta_3\frac{h_\theta}{h_r}\frac{\partial(V_{\theta j}h_\theta^{-1})}{\partial r} + (2\eta_4 - \eta_3)f_p\frac{R}{h_r}\frac{\partial(V_{\phi j}R^{-1})}{\partial r} - \eta_1(RB_\theta)^{-1}\frac{1}{h_\theta}\frac{\partial(RB_\theta V_{\theta j})}{\partial\theta} + (\eta_1 - 2\eta_2)f_p\frac{R}{h_\theta}\frac{\partial(V_{\phi j}R^{-1})}{\partial\theta}, \tag{A12}$$

$$\Pi_{\theta\phi} = \Pi_{\phi\theta} = -\frac{3}{2}\eta_0 f_p A_0 - \eta_2 R\frac{1}{h_\theta}\frac{\partial(V_{\phi j}R^{-1})}{\partial\theta} + \eta_4 R\frac{1}{h_r}\frac{\partial(V_{\phi j}R^{-1})}{\partial r}, \tag{A13}$$

$$\Pi_{\phi\phi} = -\eta_0 A_0 + 2\eta_2 f_p\frac{R}{h_\theta}\frac{\partial(V_{\phi j}R^{-1})}{\partial\theta} - 2\eta_4 f_p\frac{R}{h_r}\frac{\partial(V_{\phi j}R^{-1})}{\partial r}. \tag{A14}$$

With these, the viscous force terms in general curvilinear geometry are given by

$$(\nabla\cdot\overleftrightarrow{\Pi})_\phi = \left[\frac{1}{Rh_\theta h_r}\frac{\partial}{\partial r}(Rh_\theta\Pi_{r\phi}) + \frac{1}{Rh_r}\frac{\partial R}{\partial r}\Pi_{r\phi}\right] + \left[\frac{B_\theta}{h_\theta}\frac{\partial}{\partial\theta}\left(\frac{\Pi_{\theta\phi}}{B_\theta}\right) + \frac{1}{Rh_\theta}\frac{\partial R}{\partial\theta}\Pi_{\theta\phi}\right], \quad \text{(A15)}$$

$$(\nabla\cdot\overleftrightarrow{\Pi})_\theta = \frac{1}{H}\frac{\partial}{\partial r}(Rh_\theta\Pi_{r\theta}) + \frac{1}{H}\frac{\partial}{\partial\theta}(h_r h_\phi\Pi_{\theta\theta}) - \frac{1}{h_\theta h_r}\frac{\partial h_r}{\partial\theta}\Pi_{rr} + \frac{1}{h_\theta h_r}\frac{\partial h_\theta}{\partial r}\Pi_{\theta r} - \frac{1}{Rh_\theta}\frac{\partial R}{\partial\theta}\Pi_{\phi\phi}, \quad \text{(A16)}$$

$$(\nabla\cdot\overleftrightarrow{\Pi})_r = \frac{1}{H}\frac{\partial}{\partial r}(Rh_\theta\Pi_{rr}) + \frac{1}{H}\frac{\partial}{\partial\theta}(h_r h_\phi\Pi_{\theta r}) + \frac{1}{h_\theta h_r}\frac{\partial h_r}{\partial\theta}\Pi_{r\theta} - \frac{1}{h_\theta h_r}\frac{\partial h_\theta}{\partial r}\Pi_{\theta\theta} - \frac{1}{Rh_r}\frac{\partial R}{\partial r}\Pi_{\phi\phi}, \quad \text{(A17)}$$

where $H \equiv h_r h_\theta h_\phi$.

We note that we are retaining and representing explicitly all of the terms in both the inertial and gyroviscous tensors, rather than taking advantage of any cancellations. In fact, the derivations of 'gyroviscous cancellation' (e.g. [28]) do not seem to allow for poloidal asymmetries in flows and densities, while the gyroviscosity of this paper are caused almost entirely by these poloidal asymmetries.

The inclusion of poloidal asymmetries in flow and velocity and their calculation, and the use of the Miller equilibrium model, requires a different of type of 'ordering', because some terms must be evaluated numerically and because there is no single 'small parameter' applicable to all terms in all equations. We instead chose a three-step ordering process. In step #1, each individual term in a given equation was ordered using the appropriate ordering parameter for that term, in order to ensure that the largest contributions to that term were retained. In step #2, the various terms in a given equation were compared and smaller terms were dropped, if appropriate. Finally, in step #3, the different equations were normalized and terms with higher order nonlinearities in small unknowns were initially suppressed in order to avoid numerical difficulties in solving the coupled set of eight nonlinear equations. We have found that this approach both is necessary to obtain solutions to the coupled non-linear equations and leads to better accuracy (lower residuals) than attempting a common ordering of all terms in all equations using a generic small parameter (i.e. assuming that all small parameters are the 'same degree of small').

Appendix B. Revised circular model formalism

Continuity equation (cosine and sine moments):

$$\widetilde{V}^{\rm s}_{\theta j} = -\widetilde{n}^{\rm s}_j, \quad \text{(B1)}$$

$$\widetilde{V}^{\rm c}_{\theta j} = -(1+\widetilde{n}^{\rm c}_j). \quad \text{(B2)}$$

Electron poloidal momentum balance equation (cosine and sine moments):

$$\widetilde{\Phi}^{\rm c,s} = T_{\rm e}\widetilde{n}^{\rm c,s}_{\rm e}/\overline{\Phi}e. \quad \text{(B3)}$$

Radial momentum balance equation (1, cosine and sine moments):

$$\widehat{\Phi}^{'}_j = \frac{\overline{\Phi}^{'}}{V_{{\rm th}j}} \equiv \frac{1}{V_{{\rm th}j}\overline{B}_\theta}\frac{\partial\overline{\Phi}}{\partial r} = -\frac{\overline{E}_r}{V_{{\rm th}j}\overline{B}_\theta} = \widehat{V}_{\theta j} - \widehat{V}_{\phi j} - \widehat{P}^{'}_j, \quad \text{(B4)}$$

$$\widetilde{V}^{\rm c}_{\phi j} = 1 - \frac{\widehat{V}_{\theta j}}{\widehat{V}_{\phi j}}(\widetilde{\Phi}^{\rm c} + 2 + \widetilde{n}^{\rm c}_j) + \widetilde{\Phi}^{\rm c}\left(1 + \frac{\widehat{P}^{'}_j}{\widehat{V}_{\phi j}}\right), \quad \text{(B5)}$$

$$\widetilde{V}^{\rm s}_{\phi j} = -\frac{\widehat{V}_{\theta j}}{\widehat{V}_{\phi j}}(\widetilde{n}^{\rm s}_j + \widetilde{\Phi}^{\rm s}) + \left(1 + \frac{\widehat{P}^{'}_j}{\widehat{V}_{\phi j}}\right)\widetilde{\Phi}^{\rm s}. \quad \text{(B6)}$$

Poloidal momentum balance equation (1 moment):

$$\begin{aligned}&\widehat{V}^2_{\theta j}\left[\frac{1}{2}q\varepsilon f_p(\widetilde{n}^s_j + \widetilde{\Phi}^s)\right] - \widehat{V}_{\theta j}\left[\frac{1}{2}q\varepsilon f_p(\widehat{V}_{\phi j} + \widehat{P}^{'}_j)\widetilde{\Phi}^{\rm s} - q^2 f_j f_p \right.\\ &\left.\times\left(1 + \widetilde{\Phi}^{\rm c} + \frac{2}{3}\widetilde{n}^{\rm c}_j\right) + f_p\sum_{j\neq k}\overline{\nu}^*_{jk} + f_p\nu^*_{{\rm atom}\,j}\right]\\ &+\widehat{V}_{\theta k}\left(f_p\sum_{j\neq k}\overline{\nu}^*_{jk}\sqrt{\frac{m_j}{m_k}}\right) = q^2 f_j f_p(\widehat{V}_{\phi j} + \widehat{P}^{'}_j)\widetilde{\Phi}^{\rm c}\\ &+\frac{1}{4}q\varepsilon\widetilde{n}^{\rm s}_j + \frac{1}{4}q\varepsilon\overline{\overline{\Phi}}_j\widetilde{\Phi}^{\rm s} + \widehat{V}_{rj} - \langle M_{\theta j}\rangle\frac{qR_0}{\overline{n}_j m_j V^2_{{\rm th}j}}.\end{aligned} \quad \text{(B7)}$$

Poloidal momentum balance equation (cosine moment):

$$\begin{aligned}&\widetilde{n}^{\rm c}_j\left(\widehat{V}_{\theta j}\frac{1}{3\varepsilon}q^2 f_p f_j - \frac{1}{2}f_p\varepsilon\sum_{j\neq k}\overline{\nu}^*_{jk}\sqrt{\frac{m_j}{m_k}}\widehat{V}_{\theta k} + \frac{1}{2}\varepsilon\widehat{V}_{rj}\right)\\ &+\widetilde{n}^{\rm s}_j\left(-\frac{1}{2}qf^2_p\widehat{V}^2_{\theta j} + \frac{1}{4}q\right) + \widetilde{n}^{\rm c}_k\left(\frac{1}{2}f_p\varepsilon\sum_{j\neq k}\overline{\nu}^*_{jk}\widehat{V}_{\theta j}\right)\\ &= -\frac{1}{2\varepsilon}q^2 f_p f_j\widehat{V}_{\theta j} - \frac{1}{4}q\overline{\overline{\Phi}}_j\widetilde{\Phi}^{\rm s}\\ &+\frac{1}{2\varepsilon}q^2 f_p f_j(\widehat{V}_{\phi j} - \widehat{V}_{\theta j} + \widehat{P}^{'}_j)\widetilde{\Phi}^{\rm c}\\ &+\langle\cos\theta M_{\theta j}\rangle\frac{qR_0}{\overline{n}_j m_j V^2_{{\rm th}j}}.\end{aligned} \quad \text{(B8)}$$

Poloidal momentum balance equation (sine moment):

$$\begin{aligned}&\widetilde{n}^{\rm c}_j\left(\frac{1}{2}qf^2_p\widehat{V}^2_{\theta j} - \frac{1}{4}q\right) + \widetilde{n}^{\rm s}_j\left(\widehat{V}_{\theta j}\frac{1}{3\varepsilon}q^2 f_p f_j\right.\\ &\left.-\frac{1}{2}f_p\varepsilon\sum_{j\neq k}\overline{\nu}^*_{jk}\sqrt{\frac{m_j}{m_k}}\widehat{V}_{\theta k} + \frac{1}{2}\varepsilon\widehat{V}_{rj}\right)\\ &+\widetilde{n}^{\rm s}_k\left(\frac{1}{2}f_p\varepsilon\sum_{j\neq k}\overline{\nu}^*_{jk}\widehat{V}_{\theta j}\right)\\ &= -\frac{1}{2}qf^2_p\widehat{V}^2_{\theta j} - \frac{1}{2}qf_p\widehat{V}_{\theta j}\widehat{V}_{\phi j}\\ &+\frac{1}{2\varepsilon}q^2 f_p f_j(\widehat{V}_{\phi j} - \widehat{V}_{\theta j} + \widehat{P}^{'}_j)\widetilde{\Phi}^{\rm s}\\ &+\frac{1}{4}q\overline{\overline{\Phi}}_j\widetilde{\Phi}^{\rm c} + \langle\sin\theta M_{\theta j}\rangle\frac{qR_0}{\overline{n}_j m_j V^2_j}.\end{aligned} \quad \text{(B9)}$$

Angular inertial torque (moment):

$$\langle n_j m_j R^2\nabla\phi\cdot(\vec{V}_j\cdot\nabla)\vec{V}_j\rangle = R_0\overline{n}_j m_j\nu_{nj}\overline{V}_{\phi j}, \quad \text{(B10)}$$

where

$$\nu_{nj} \equiv \frac{1}{2}\frac{\overline{V}_{rj}}{R_0}[\varepsilon(1+\widetilde{n}_j^{\rm c}+\widetilde{V}_{\phi j}^{\rm c})-2R_0L_{\overline{V}_{\phi j}}^{-1}]$$
$$=\frac{1}{2}\frac{\overline{V}_{rj}}{R_0}\left\{\varepsilon\left[2+\widetilde{n}_j^{\rm c}-\frac{\widehat{V}_{\theta j}}{\widehat{V}_{\phi j}}(\widetilde{\Phi}^{\rm c}+2+\widetilde{n}_j^{\rm c})\right.\right.$$
$$\left.\left.+\,\widetilde{\Phi}^{\rm c}\left(1+\frac{\widehat{P}_j^{'}}{\widehat{V}_{\phi j}}\right)\right]-2R_0L_{\overline{V}_{\phi j}}^{-1}\right\}. \tag{B11}$$

Angular viscous torque (1 moment):

$$\langle R^2\nabla\phi\cdot\nabla\cdot\overleftrightarrow{\mathbf{\Pi}}\rangle \approx \langle(R^2\nabla\phi\cdot\nabla\cdot\overleftrightarrow{\mathbf{\Pi}})_{\rm gv}\rangle$$
$$=-\left\langle\frac{1}{Rh_\theta h_r}\frac{\partial}{\partial r}\left(R^3\eta_4\frac{\partial(V_{\phi j}R^{-1})}{\partial\theta}\right)\right\rangle$$
$$\equiv R_0\overline{n}_j m_j \nu_{{\rm d}j}\overline{V}_{\phi j}, \tag{B12}$$

where

$$\nu_{{\rm d}j}=-\frac{1}{2}\frac{T_j}{R_0^2e_j\overline{B}_\phi}(4\widetilde{V}_{\phi j}^{\rm s}+\widetilde{n}_j^{\rm s})+\frac{1}{2}\frac{\widetilde{\theta}_jG_jT_j}{R_0^2e_j\overline{B}_\phi}$$
$$=\frac{1}{2}\frac{T_j}{R_0^2e_j\overline{B}_\phi}\left[4\frac{\widehat{V}_{\theta j}}{\widehat{V}_{\phi j}}(\widetilde{n}_j^{\rm s}+\widetilde{\Phi}^{\rm s})\right.$$
$$\left.-4\left(1+\frac{\widehat{P}_j^{'}}{\widehat{V}_{\phi j}}\right)\widetilde{\Phi}^{\rm s}-\widetilde{n}_j^{\rm s}\right]+\frac{1}{2}\frac{G_j\widetilde{\theta}_jT_j}{R_0^2e_j\overline{B}_\phi}, \tag{B13}$$

$$G_j\equiv r(L_{\overline{n}_j}^{-1}+L_{T_j}^{-1}+L_{\overline{V}_\phi}^{-1}), \tag{B14}$$

$$\widetilde{\theta}_j\equiv\widetilde{V}_{\phi j}^{\rm s}(4+\widetilde{n}_j^{\rm c})+\widetilde{n}_j^{\rm s}(1-\widetilde{V}_{\phi j}^{\rm c})$$
$$=(4+\widetilde{n}_j^{\rm c})\left[-\frac{\widehat{V}_{\theta j}}{\widehat{V}_{\phi j}}(\widetilde{n}_j^{\rm s}+\widetilde{\Phi}^{\rm s})+\left(1+\frac{\widehat{P}_j^{'}}{\widehat{V}_{\phi j}}\right)\widetilde{\Phi}^{\rm s}\right]$$
$$+\widetilde{n}_j^{\rm s}\left[\frac{\widehat{V}_{\theta j}}{\widehat{V}_{\phi j}}(\widetilde{\Phi}^{\rm c}+2+\widetilde{n}_j^{\rm c})-\widetilde{\Phi}^{\rm c}\left(1+\frac{\widehat{P}_j^{'}}{\widehat{V}_{\phi j}}\right)\right]. \tag{B15}$$

Toroidal angular momentum balance equation (1 moment):

$$\overline{n}_jm_j\sum_{j\neq k}\overline{\nu}_{jk}\left[\left(1+\frac{\nu_{nj}+\nu_{{\rm d}j}+S_{{\rm nb}j}/\overline{n}_j}{\sum_{j\neq k}\overline{\nu}_{jk}}\right)\overline{V}_{\phi j}-\overline{V}_{\phi k}\right]$$
$$=\overline{n}_je_jE_\phi^A+e_j\Gamma_{rj}\overline{B}_\theta+\overline{M}_{\phi j}. \tag{B16}$$

Appendix C. Coefficients in the Miller model formalism

Radial momentum balance equation (cosine moment):

$$\alpha_j^{1S}\equiv-\frac{\left\langle\sin^2\theta\frac{1}{h_r}\right\rangle}{\left(1+\frac{\partial R_0(r)}{\partial r}\right)\left\langle\frac{\sin^2\theta}{(1+\varepsilon\cos\xi)}\frac{1}{h_r}\right\rangle}$$
$$\times\left(\frac{\widehat{\Phi}_j^{'}}{\widehat{V}_{\phi j}}+\frac{\widehat{P}_j^{'}}{\widehat{V}_{\phi j}}+1\right),$$
$$\alpha_j^{2S}\equiv-\frac{\widehat{\Phi}_j^{'}}{\widehat{V}_{\phi j}}\widetilde{\Phi}^s\frac{\left\langle\sin^2\theta\frac{1}{h_r}\right\rangle}{\left(1+\frac{\partial R_0(r)}{\partial r}\right)\left\langle\frac{\sin^2\theta}{(1+\varepsilon\cos\xi)}\frac{1}{h_r}\right\rangle} \tag{C1}$$

Radial momentum balance equation (sine moment):

$$\alpha_j^{1C}\equiv-\frac{1}{\varepsilon}\frac{\left\langle\frac{\cos\theta}{(1+\varepsilon\cos\xi)}\frac{1}{h_r}\right\rangle+\varepsilon\widetilde{n}_j^c\left\langle\frac{\cos^2\theta}{(1+\varepsilon\cos\xi)}\frac{1}{h_r}\right\rangle}{\left\langle\frac{\cos^2\theta}{(1+\varepsilon\cos\xi)}\frac{1}{h_r}\right\rangle},$$
$$\alpha_j^{2C}\equiv-\frac{1}{\varepsilon}\frac{\left\langle\cos\theta\frac{1}{h_r}\right\rangle+\varepsilon(\widetilde{n}_j^{\rm c}+\widetilde{\Phi}^{\rm c})\left\langle\cos^2\theta\frac{1}{h_r}\right\rangle}{\left(1+\frac{\partial R_0(r)}{\partial r}\right)\left\langle\frac{\cos^2\theta}{(1+\varepsilon\cos\xi)}\frac{1}{h_r}\right\rangle},$$
$$\alpha_j^{3C}\equiv\frac{1}{\varepsilon}\frac{\left\langle\frac{\cos\theta}{1+\varepsilon\cos\xi}\right\rangle+\frac{\left\langle\frac{1}{R}\frac{\partial R}{\partial\theta}\sin\theta\frac{1}{h_\theta}\right\rangle}{\left\langle\sin^2\theta\frac{1}{h_\theta}\right\rangle}\left\langle\frac{\cos^2\theta}{1+\varepsilon\cos\xi}\right\rangle}{\left(1+\frac{\partial R_0(r)}{\partial r}\right)\left\langle\frac{\cos^2\theta}{(1+\varepsilon\cos\xi)}\frac{1}{h_r}\right\rangle},$$
$$\alpha_j^{4C}\equiv-\frac{1}{\varepsilon}\frac{\left\langle\cos\theta\frac{1}{h_r}\right\rangle+\varepsilon\widetilde{n}_j^{\rm c}\left\langle\cos^2\theta\frac{1}{h_r}\right\rangle}{\left(1+\frac{\partial R_0(r)}{\partial r}\right)\left\langle\frac{\cos^2\theta}{(1+\varepsilon\cos\xi)}\frac{1}{h_r}\right\rangle}. \tag{C2}$$

Poloidal momentum balance equation (1 moment):

$$A_{11}=qrf_p^2\widetilde{n}_j^{\rm s}\left(\left\langle\frac{\cos\theta}{h_\theta}\right\rangle+\frac{\left\langle\frac{1}{R}\frac{\partial R}{\partial\theta}\frac{\sin\theta}{h_\theta}\right\rangle}{\left\langle\frac{\sin^2\theta}{h_\theta}\right\rangle}\left\langle\frac{\cos^2\theta}{h_\theta}\right\rangle\right),$$

$$A_{12}=-q^2R_0^2f_pf_j$$
$$\times\left\{\begin{array}{l}\widetilde{n}_j^{\rm c}\varepsilon\left[-\frac{1}{3}\frac{\left\langle\frac{1}{R}\frac{\partial R}{\partial\theta}\sin\theta\frac{1}{h_\theta}\right\rangle}{\left\langle\frac{\sin^2\theta}{h_\theta}\right\rangle}\left(\left\langle\frac{\sin^2\theta}{(h_\theta)^2}\right\rangle-\left\langle\frac{\cos^2\theta}{(h_\theta)^2}\right\rangle\right)\right.\\ \quad+\frac{1}{3}\left\langle\frac{\partial h_\theta}{\partial\theta}\frac{\sin\theta}{(h_\theta)^3}\right\rangle-\left\langle\frac{1}{R}\frac{\partial R}{\partial\theta}\frac{\sin\theta}{(h_\theta)^2}\right\rangle-\frac{1}{3}\left\langle\frac{\cos\theta}{(h_\theta)^2}\right\rangle\Big]\\ +3\langle Q\rangle+\langle M\rangle+\frac{\left\langle\frac{1}{R}\frac{\partial R}{\partial\theta}\sin\theta\frac{1}{h_\theta}\right\rangle}{\left\langle\frac{\sin^2\theta}{h_\theta}\right\rangle}\\ \times\left(-\frac{1}{3}\left\langle\frac{\partial h_\theta}{\partial\theta}\frac{\sin\theta}{(h_\theta)^3}\right\rangle+\left\langle\frac{1}{R}\frac{\partial R}{\partial\theta}\frac{\sin\theta}{(h_\theta)^2}\right\rangle\right.\\ \left.+\frac{1}{3}\left\langle\frac{\cos\theta}{(h_\theta)^2}\right\rangle+\langle M\cos\theta\rangle-\langle P\sin\theta\rangle\right)\end{array}\right\}$$
$$+qrf_p\widehat{V}_{\phi j}\widetilde{V}_\phi^{\rm s}\left\langle\frac{1}{R}\frac{\partial R}{\partial\theta}\frac{\sin\theta}{h_\theta}\right\rangle-f_p\sum_{j\neq k}\overline{\nu}_{jk}^*-f_p\nu_{{\rm atom}\,j}^*,$$

$$A_{13}=f_p\sum_{j\neq k}\overline{\nu}_{jk}^*\sqrt{\frac{m_j}{m_k}},$$

$$B_1=\widehat{V}_{\phi j}\widetilde{V}_{\phi j}^{\rm c}q^2R_0^2f_jf_p\varepsilon\left(\left\langle\frac{\partial h_\theta}{\partial\theta}\frac{\sin\theta}{(h_\theta)^3}\right\rangle-\left\langle\frac{\cos\theta}{(h_\theta)^2}\right\rangle\right.$$
$$\left.-\langle N\cos\theta\rangle-2\left\langle\frac{1}{R}\frac{\partial R}{\partial\theta}\frac{\sin\theta}{(h_\theta)^2}\right\rangle\right)$$
$$+\widehat{V}_{\phi j}q^2R_0^2f_jf_p\left[\varepsilon\widetilde{n}_j^{\rm c}\left(\left\langle\frac{1}{R}\frac{\partial R}{\partial\theta}\sin\theta\frac{1}{(h_\theta)^2}\right\rangle\right.\right.$$
$$\left.\left.-\langle N\cos\theta\rangle\right)-\langle N\rangle-3\left\langle\left(\frac{1}{R}\frac{\partial R}{\partial\theta}\right)^2\frac{1}{(h_\theta)^2}\right\rangle\right]$$

$$+\frac{1}{2}qr\widetilde{n}^{\rm s}_j\left\langle\frac{\cos\theta}{h_\theta}\right\rangle-\langle M_{\theta j}\rangle\frac{qR_0}{\overline{n}_j m_j V^2_{thj}}$$
$$+\widehat{V}_{rj}\left\langle\frac{1}{(1+\varepsilon\cos\xi)}\right\rangle+\frac{1}{2}qr\varepsilon\overline{\overline{\Phi}}_j\left[\widetilde{\Phi}^{\rm s}\left(\frac{1}{\varepsilon}\left\langle\frac{\cos\theta}{h_\theta}\right\rangle\right.\right.$$
$$\left.\left.+\widetilde{n}^{\rm c}_j\left\langle\frac{\cos^2\theta}{h_\theta}\right\rangle\right)-\widetilde{n}^{\rm s}_j\widetilde{\Phi}^{\rm c}\left\langle\frac{\sin^2\theta}{h_\theta}\right\rangle\right], \tag{C3}$$

where

$$N\equiv-\left(\frac{1}{R}\frac{\partial R}{\partial\theta}\right)^2\frac{1}{(h_\theta)^2}-\frac{\partial h_\theta}{\partial\theta}\frac{1}{R}\frac{\partial R}{\partial\theta}\frac{1}{(h_\theta)^3}+\frac{1}{R}\frac{\partial^2 R}{\partial\theta^2}\frac{1}{(h_\theta)^2},$$
$$M\equiv N+\frac{1}{3}\left[-\left(\frac{1}{B_\theta}\frac{\partial B_\theta}{\partial\theta}\right)^2\frac{1}{(h_\theta)^2}-\frac{\partial h_\theta}{\partial\theta}\frac{1}{B_\theta}\frac{\partial B_\theta}{\partial\theta}\frac{1}{(h_\theta)^3}\right.$$
$$\left.+\frac{1}{B_\theta}\frac{\partial^2 B_\theta}{\partial\theta^2}\frac{1}{(h_\theta)^2}\right]$$
$$P\equiv\frac{1}{R}\frac{\partial R}{\partial\theta}\frac{1}{(h_\theta)^2}+\frac{1}{3}\frac{1}{B_\theta}\frac{\partial B_\theta}{\partial\theta}\frac{1}{(h_\theta)^2},$$
$$Q\equiv\left(\frac{1}{R}\frac{\partial R}{\partial\theta}\right)^2\frac{1}{(h_\theta)^2}+\frac{1}{3}\left(\frac{1}{R}\frac{\partial R}{\partial\theta}\right)\left(\frac{1}{B_\theta}\frac{\partial B_\theta}{\partial\theta}\right)\frac{1}{(h_\theta)^2},$$
$$\widehat{V}_{rj}\equiv\frac{qR_0e_j\overline{B}_\phi}{m_jV^2_{thj}}\overline{V}_{rj},\ \text{and}\ \overline{\overline{\Phi}}_j\equiv\frac{e_j\overline{\Phi}}{\frac{1}{2}m_jV^2_{thj}}=\frac{e_j\overline{\Phi}}{T_j}=\frac{Z_je\overline{\Phi}}{T_j}.$$

Poloidal momentum balance equation (cosine moment):

$$A_{C1}=q^2R_0rf_jf_p\left[-\widehat{V}_{\theta j}\frac{1}{3}\left(-\left\langle\frac{\partial h_\theta}{\partial\theta}\frac{\sin\theta\cos\theta}{(h_\theta)^3}\right\rangle\right.\right.$$
$$\left.+\left\langle\frac{\cos^2\theta}{(h_\theta)^2}\right\rangle\right)-\widehat{V}_{\phi j}\langle N\cos^2\theta\rangle$$
$$-\sum_{j\neq k}\overline{\nu}^*_{jk}\varepsilon f_p\sqrt{\frac{m_j}{m_k}}\widehat{V}_{\theta k}\langle\cos^2\theta\rangle$$
$$\left.-\widehat{V}_{rj}\varepsilon\left\langle\frac{\cos^2\theta}{(1+\varepsilon\cos\xi)}\right\rangle\right],$$
$$A_{C2}=qr\left(-f_p^2\widehat{V}^2_{\theta j}\left\langle\cos^2\theta\frac{1}{h_\theta}\right\rangle+\frac{1}{2}\left\langle\frac{\cos^2\theta}{h_\theta}\right\rangle\right),$$
$$A_{C3}=\sum_{j\neq k}\overline{\nu}^*_{jk}\varepsilon f_p\widehat{V}_{\theta j}\langle\cos^2\theta\rangle,$$

$$B_C=qrf_p\widehat{V}_{\theta j}\widehat{V}_{\phi j}\widetilde{V}^{\rm s}_\phi\left\langle\frac{1}{R}\frac{\partial R}{\partial\theta}\sin\theta\cos\theta\frac{1}{h_\theta}\right\rangle$$
$$-\widehat{V}_{\theta j}q^2R_0^2f_jf_p\left[\frac{\left\langle\frac{1}{R}\frac{\partial R}{\partial\theta}\frac{\sin\theta}{h_\theta}\right\rangle}{\left\langle\frac{\sin^2\theta}{h_\theta}\right\rangle}\right.$$
$$\times\left(-\frac{1}{3}\left\langle\frac{\partial h_\theta}{\partial\theta}\frac{\sin\theta\cos\theta}{(h_\theta)^3}\right\rangle\right.$$
$$\left.\left.+\frac{1}{3}\left\langle\frac{\cos^2\theta}{(h_\theta)^2}\right\rangle+\langle M\cos^2\theta\rangle-\langle P\sin\theta\cos\theta\rangle\right)\right.$$
$$\left.+\langle M\cos\theta\rangle+3\langle Q\cos\theta\rangle\right]$$
$$-\widehat{V}_{\phi j}\widetilde{V}^{\rm c}_{\phi j}q^2R_0rf_jf_p\left(\left\langle\frac{\partial h_\theta}{\partial\theta}\frac{\sin\theta\cos\theta}{(h_\theta)^3}\right\rangle-\left\langle\frac{\cos^2\theta}{(h_\theta)^2}\right\rangle\right.$$
$$\left.-\langle N\cos^2\theta\rangle\right)-\widehat{V}_{\phi j}q^2R_0^2f_jf_p\langle N\cos\theta\rangle$$
$$+\langle\cos\theta M_{\theta j}\rangle\frac{qR_0}{\overline{n}_jm_jV^2_{{\rm th}j}}$$
$$-\sum_{j\neq k}\overline{\nu}^*_{jk}f_p\left(\widehat{V}_{\theta j}-\sqrt{\frac{m_j}{m_k}}\widehat{V}_{\theta k}\right)$$
$$\times\left(\langle\cos\theta\rangle+\frac{\left\langle\frac{1}{R}\frac{\partial R}{\partial\theta}\frac{\sin\theta}{h_\theta}\right\rangle}{\left\langle\frac{\sin^2\theta}{h_\theta}\right\rangle}\langle\cos^2\theta\rangle\right)$$
$$-\widehat{V}_{rj}\left\langle\frac{\cos\theta}{(1+\varepsilon\cos\xi)}\right\rangle-\frac{1}{2}qr\overline{\overline{\Phi}}_j\widetilde{\Phi}^{\rm s}\left\langle\frac{\cos^2\theta}{h_\theta}\right\rangle$$
$$-f_p\nu^*_{{\rm atom}\,j}\widehat{V}_{\theta j}\left(\langle\cos\theta\rangle+\frac{\left\langle\frac{1}{R}\frac{\partial R}{\partial\theta}\frac{\sin\theta}{h_\theta}\right\rangle}{\left\langle\frac{\sin^2\theta}{h_\theta}\right\rangle}\langle\cos^2\theta\rangle\right). \tag{C4}$$

Poloidal momentum balance equation (sine moment):

$$A_{S1}=qrf_p^2\widehat{V}^2_{\theta j}\left\langle\sin^2\theta\frac{1}{h_\theta}\right\rangle-\frac{1}{2}qr\left\langle\frac{\sin^2\theta}{h_\theta}\right\rangle,$$
$$A_{S2}=q^2R_0rf_jf_p\left[-\widehat{V}_{\theta j}\frac{1}{3}\left(\left\langle\frac{\partial h_\theta}{\partial\theta}\frac{\sin\theta\cos\theta}{(h_\theta)^3}\right\rangle+\left\langle\frac{\sin^2\theta}{(h_\theta)^2}\right\rangle\right.\right.$$
$$\left.\left.+\langle P\sin\theta\cos\theta\rangle\right)-\widehat{V}_{\phi j}3\left\langle\left(\frac{1}{R}\frac{\partial R}{\partial\theta}\right)^2\frac{\sin^2\theta}{(h_\theta)^2}\right\rangle\right]$$
$$-\varepsilon\sum_{j\neq k}\overline{\nu}^*_{jk}f_p\sqrt{\frac{m_j}{m_k}}\widehat{V}_{\theta k}\langle\sin^2\theta\rangle+\widehat{V}_{rj}\varepsilon\left\langle\frac{\sin^2\theta}{(1+\varepsilon\cos\xi)}\right\rangle,$$
$$A_{S3}=\varepsilon\sum_{j\neq k}\overline{\nu}^*_{jk}f_p\widehat{V}_{\theta j}\langle\sin^2\theta\rangle,$$

$$B_S=qrf_p^2\widehat{V}^2_{\theta j}\frac{1}{\varepsilon}\left\langle\frac{1}{R}\frac{\partial R}{\partial\theta}\sin\theta\frac{1}{h_\theta}\right\rangle$$
$$+qrf_p\widehat{V}_{\theta j}\widehat{V}_{\phi j}\frac{1}{\varepsilon}\left\langle\frac{1}{R}\frac{\partial R}{\partial\theta}\sin\theta\frac{1}{h_\theta}\right\rangle$$
$$-\widehat{V}_{\phi j}\widetilde{V}^s_{\phi j}q^2R_0rf_jf_p\left[-\left\langle\frac{\partial h_\theta}{\partial\theta}\frac{\sin\theta\cos\theta}{(h_\theta)^3}\right\rangle-\left\langle\frac{\sin^2\theta}{(h_\theta)^2}\right\rangle\right.$$
$$\left.-3\left\langle\left(\frac{1}{R}\frac{\partial R}{\partial\theta}\right)^2\frac{\sin^2\theta}{(h_\theta)^2}\right\rangle\right]$$
$$+\left\langle\sin\theta M_{\theta j}\right\rangle\frac{qR_0}{\overline{n}_jm_jV^2_{{\rm th}j}}+\frac{1}{2}qr\overline{\overline{\Phi}}_j\widetilde{\Phi}^c\left\langle\frac{\sin^2\theta}{h_\theta}\right\rangle. \tag{C5}$$

References

[1] Stacey W.M., Bailey A.W., Sigmar D.J. and Shaing K.C. 1985 *Nucl. Fusion* **25** 463
[2] Burrell K.H., Ohkawa T. and Wong S.K. 1981 *Phys. Rev. Lett.* **47** 511
[3] Bondeson A. and Ward D.J. 1994 *Phys. Rev. Lett.* **72** 2709
[4] Garofalo A.M. *et al* and DIII-D Team 2001 *Nucl. Fusion* **41** 1171
[5] Burrell K.H. 1997 *Phys. Plasmas* **4** 1499
[6] deGrassie J.S., Baker D.R., Burrell K.H., Gohil P., Greenfield C.M., Groebner R.J. and Thomas D.M. 2003 *Nucl. Fusion* **43** 142

[7] Zastrow K.D., Core W.G.F., Eriksson L.G., Von Hellermann M.G., Howman A.C. and Konig R.W.T. 1998 *Nucl. Fusion* **38** 257
[8] Scott S.D. *et al* 1990 *Phys. Fluids* B **2** 1300
[9] Suckewer S., Eubank H.P., Goldston R.J., Hinnov E. and Sauthoff N.R. 1979 *Phys. Rev. Lett.* **43** 207
[10] Isler R.C. *et al* 1983 *Nucl. Fusion* **23** 1017
[11] Groebner R.J., Pfeiffer W., Blau F.P., Burrell K.H., Fairbanks E.S., Seraydarian R.P., Stjohn H. and Stockdale R.E. 1986 *Nucl. Fusion* **26** 543
[12] Stacey W.M. 2008 *Phys. Plasmas* **15** 012501
[13] Kaufman A.N. 1960 *Phys. Fluids* **3** 610
[14] Braginskii S.I. 1965 *Rev. Plasma Phys.* **1** 205
[15] Hazeltine R.D. 1974 *Phys. Fluids* **17** 961
[16] Tsang K.T. and Frieman E.A. 1976 *Phys. Fluids* **19** 747
[17] Mikhailovskii A.B. and Tsypin V.S. 1984 *Sov. J. Plasma Phys.* **10** 51
[18] Stacey W.M. and Sigmar D.J. 1985 *Phys. Fluids* **28** 2800
[19] Hinton F.L. and Wong S.K. 1985 *Phys. Fluids* **28** 3082
[20] Connor J.W., Cowley S.C., Hastie R.J. and Pan L.R. 1987 *Plasma Phys. Control. Fusion* **29** 919
[21] Stacey W.M. 1992 *Phys. Fluids* B **4** 3302
[22] Hazeltine R.D. and Meiss J.D. 1994 *Plasma Confinement* (Reading, MA: Addison-Wesley) p 208, 220 and 226
[23] Rogister A. 1994 *Phys. Plasmas* **1** 619
[24] Claassen H.A., Gerhauser H., Rogister A. and Yarim C. 2000 *Phys. Plasmas* **7** 3699
[25] Stacey W.M. 2004 *Phys. Plasmas* **11** 3096
[26] Wong S.K. and Chan V.S. 2004 *Phys. Plasmas* **11** 3432
[27] Catto P.J. and Simakov A.N. 2005 *Phys. Plasmas* **12** 012501
[28] Ramos J.J. 2005 *Phys. Plasmas* **12** 112301
[29] Catto P.J. and Simakov A.N. 2004 *Phys. Plasmas* **11** 90
[30] Stacey W.M., Johnson R.W. and Mandrekas J. 2006 *Phys. Plasmas* **13** 062508
[31] Stacey W.M. and Jackson D.R. 1993 *Phys. Fluids* B **5** 1828
[32] Stacey W.M. and Murakami M. 2001 *Phys. Plasmas* **8** 4450
[33] Stacey W.M. and Mandrekas J. 2002 *Phys. Plasmas* **9** 1622
[34] Miller R.L., Chu M.S., Greene J.M., Lin-Liu Y.R. and Waltz R.E. 1998 *Phys. Plasmas* **5** 973
[35] Stacey W.M. 2008 *Phys. Plasmas* **15** 122505
[36] Stacey W.M. and Bae C. 2009 *Phys. Plasmas* **16** 082501
[37] Luxon J.L. 2002 *Nucl. Fusion* **42** 614
[38] Hirshman S.P. and Sigmar D.J. 1981 *Nucl. Fusion* **21** 1079
[39] Houlberg W.A., Shaing K.C., Hirshman S.P. and Zarnstorff M.C. 1997 *Phys. Plasmas* **4** 3230
[40] Kim Y.B., Diamond P.H. and Groebner R.J. 1991 *Phys. Fluids* B **3** 2050
[41] Stacey W.M. 2002 *Phys. Plasmas* **9** 3874
[42] Stacey W.M. 2005 *Fusion Plasma Physics* (Weinheim: Wiley-VCH) pp 251–66
[43] Candy J. 2009 *Plasma Phys. Control. Fusion* **51** 105009
[44] Stacey W.M. 2008 *Contrib. Plasma Phys.* **48** 94
[45] Stacey W.M. and Groebner R.J. 2008 *Phys. Plasmas* **15** 012503
[46] Solomon W.M., Burrell K.H., Gohil P., Groebner R.J. and Baylor L.R. 2004 *Rev. Sci. Instrum.* **75** 3481
[47] Solomon W.M., Burrell K.H., Feder R., Nagy A., Gohil P. and Groebner R.J. 2008 *Rev. Sci. Instrum.* **79** 10F531
[48] Solomon W.M., Burrell K.H., Andre R., Baylor L.R., Budny R., Gohil P., Groebner R.J., Holcomb C.T., Houlberg W.A. and Wade M.R. 2006 *Phys. Plasmas* **13** 056116
[49] Grierson B.A., Burrell K.H., Solomon W.M. and Pablant N.A. 2010 *Rev. Sci. Instrum.* **81**
[50] Chapman S. and Cowling T.G. 1939 *The Mathematical Theory on Non-Uniform Gases* (Cambridge: Cambridge University Press)